Hindawi
Complexity
Volume 2023, Article ID 9066127, 24 pages
https://doi.org/10.1155/2023/9066127

Research Article

Modeling and Simulation Analysis of Bionic Flapping-Wing Flight Attitude Control Based on L1 Adaptive

Lun Li[1,2], **Fan Bai**[3], **Wencheng Wang**[1,2], **Xiaojin Wu**[1,2] **and Yihua Dong**[1,2]

[1]*Institute of Machinery and Automation, Weifang University, Weifang 261061, China*
[2]*University Engineering Research Center for Robot Vision Perception and Control, Weifang 261061, China*
[3]*School of Equipment Engineering, Shenyang Polytechnic University, Shenyang 110159, China*

Correspondence should be addressed to Lun Li; ll408907652@163.com

Received 3 January 2023; Revised 3 September 2023; Accepted 16 September 2023; Published 4 October 2023

Academic Editor: Dan Selişteanu

Flapping-wing flight control is a multi-input and multi-output nonlinear system with uncertainties, which is affected by modeling errors, parameter variations, external disturbances, and unmodeled dynamics. Parameter uncertainty has a great impact on the stability control of flapping-wing flight, and gain adjustment is a common means to deal with parameter uncertainty, but it is complex and time-consuming. Based on the mechanism of flapping-wing flight, a nonlinear dynamic model for flapping-wing dynamic flight is established by analyzing the forces, moments, and attitude changes of the fuselage and wing in detail. Based on the constructed dynamic model, a fast robust adaptive flapping-wing flight control method is proposed. The state predictor is designed to estimate and monitor the uncertain parameters in the flapping-wing attitude control model, and the adaptive law adjusts the parameter estimation to ensure that the output error between the state predictor and the controlled object is stable in the Lyapunov sense, and finally the adaptive control law is obtained. At the same time, the Monte Carlo-support vector machine method is used to optimize the boundary of the control parameters in the flight control to obtain the control parameters that can meet the control expectations, and the obtained parameters are classified and judged according to the stable level flight conditions. Based on the adjusted parameters and the predetermined control signal, the control amount is adjusted according to the control law. When the adaptive gain is large enough, the simulation results show that the system has good transient response characteristics.

1. Introduction

Flapping-wing flight control is a typical high-order uncertain nonlinear control problem. Flapping wing relies on the rapid flapping of wings to generate the power needed for flight, and the aircraft itself needs to use flexible lightweight materials to improve flight efficiency. However, the flexible lightweight fuselage is easily disturbed by external forces, resulting in unstable flight. At the same time, the rapid flapping of the wing during flapping flight will cause greater vibration of the whole system, and its own vibration and external disturbance will cause the performance of sensors and actuators to decline and the measurement error of motion parameters to increase. Therefore, the flapping-wing flight control needs a control algorithm that matches the flapping-wing flight characteristics to achieve its system stability [1].

Traditional flight control algorithms of fixed wing and rotor cannot meet the control requirements of flapping-wing flight. The unsteady and strong coupling characteristics of flapping-wing flight bring great challenges to the modeling and control of bionic flapping-wing flight robots. At the same time, the application environment of bionic ornithopter with limited load capacity and unstructured and multi-interference further aggravates the complexity and difficulty of autonomous flight control of bionic ornithopter.

In order to solve the nonlinear and unsteady flight control problem of flapping wing, many scholars at home and abroad have studied it. Based on the hummingbird model, He [2] et al. used full-state feedback neural network

control and output feedback neural network, respectively, to adjust the attitude of the ornithopter. The neural network was used to estimate the uncertainty in the model, and the disturbance observer was designed to eliminate the influence of interference. Cheng and Deng [3] adopted a neural network model to approximate the nonlinear model of the insect-like flapping-wing flight robot, parameterized the wing kinematics model of the flying robot, and designed a neural adaptive controller to control the attitude angle of the insect-like flapping-wing flight robot. The asymptotic convergence of system output is proved based on Lyapunov stability analysis. Rodriguez [4] and others used the ladder design method based on generalized mixed sensitivity to model and control the flapping-wing aircraft. Because the lift generated by the flapping-wing has a certain periodicity, the average theory was used to transform the nonlinear time-varying model into a nonlinear time-invariant model, and then the model was linearized under different flight conditions. A new H-infinity control method based on convex optimization is proposed to deal with various control parameters that may conflict with each other, such as the frequency and time-domain closed-loop characteristics of the input and output of the system. Chirarattananon et al. [5, 6] used the adaptive control method to model and control in order to deal with the nonlinear continuity and model uncertainty of the system in the flapping-wing flight process and successfully made the BoboBee flapping-wing aircraft hover and land. Bluman and Kang [7, 8] and others used the sliding mode control method to verify the effectiveness of two different types of sliding mode control strategies in maintaining the flapping wing hovering in the pitch plane when the flapping wing was disturbed by external wind and the wing was damaged. Tahmasian et al. [9, 10] proposed a longitudinal control method for flapping-wing aircraft. Based on the control model of conventional aircraft, the influence of wing inertia on the system model was introduced, and the vibration and feedback control were combined to control the longitudinal dynamic equation of flapping wing. Biswal et al. [11] established three nonlinear flapping-wing flight control models, and the complexity of the models is increasing. The first model contains only rigid body dynamics and ignores wing dynamics, the second model contains rigid body dynamics and wing dynamics, and the third model contains complete rigid body and rigid wing dynamics. In order to improve the accuracy of the model, the linear quadratic regulator (LQR) is used as the design method of the main control system, combined with the nonlinear parameter optimization algorithm, and the flapping-wing flight control algorithm is given.

Through the above analysis, with the continuous deepening of research on autonomous flight control technology of bionic flapping-wing aircraft, a variety of control methods have been applied to the flight control system of bionic flapping-wing aircraft, including PID control, linear quadratic control, fuzzy control, genetic algorithm control, neural network control, and adaptive control. However, the traditional PID control parameters cannot be adjusted according to the actual flight state of the ornithopter due to the characteristics of unsteady, strong coupling and easy to be disturbed by environment. Although the intelligent control methods such as fuzzy control, genetic algorithm control, and neural network control have the advantage of less dependence on the precise parameters of the control model, their control systems are difficult to be described by accurate mathematical methods, and it is difficult to optimize the controller by system analysis methods. The adaptive control method relies less on the internal model parameters and external interference information of the system, can gradually improve the control during the operation of the system, and has certain adaptability. In this paper, based on the model reference adaptive control algorithm, a low-pass filter is introduced to filter the high-frequency vibration signal and then reduce the oscillation of the control law, so that it has good adaptability and good robustness.

Based on the prototype of the bionic ornithopter system, the flight dynamics modeling of the ornithopter is carried out in this paper. On this basis, a fast and robust adaptive control (L1AC) method is used to estimate and monitor the uncertain parameters in the attitude control model of the flapping wing by designing a state predictor, and the parameter estimation is adjusted by the adaptive law, so as to ensure that the output error between the state predictor and the controlled object is stable in the Lyapunov sense, and finally the adaptive control law is obtained. At the same time, the Monte Carlo-support vector machine method is used to optimize the boundary of control parameters in flight control, and the control parameters that can meet the control expectations are obtained. The obtained parameters are classified according to the stable level flight conditions, and the designed controller and optimization algorithm are verified by simulation.

2. Flapping-Wing Flight Mechanism and Aerodynamic Force Generation Mechanism

Wings are the main organs for birds to generate lift, and the movement mode of wings is an important part of the research on the aerodynamic force generation mode of flapping wings. Depending on the movement of wings, birds can take off, land, turn sharply, hover, level flight, and perform other flight movements, and the way of wing movement is different for different movements. Generally speaking, there are four basic modes of bird wing movement: flapping up and down, twisting in the chord direction, swinging back and forth, and bending in the span direction [12, 13], as shown in Figure 1. Flapping up and down is the main action of wing movement, which can generate upward lift force, which mainly overcomes its own gravity to achieve flight. Wing flapping is accompanied by chord-wise torsional motion, and the angle of attack of the wing can be timely changed according to the change of wind speed and wind direction or the need of flight attitude, which can provide part of the lift and forward thrust. At the same time, through the chord-wise twisting motion of the wings, the flight attitude can be adjusted to achieve hovering, turning, flying, and other actions. Forward and backward flapping motion is the forward and backward motion of wings in the plane of the fuselage, which is more obvious in small birds and

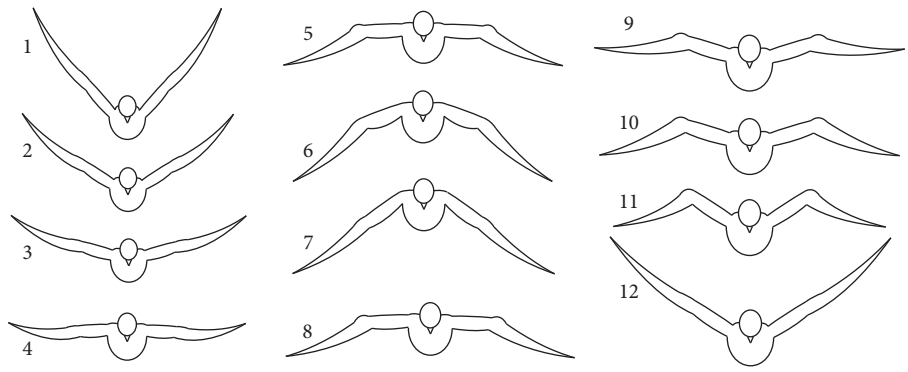

Figure 1: Breakdown of flapping action process.

insects, and can provide forward thrust during flight. In that upwelling process of the bird wings, in addition to the reduction of the pressure difference due to the fact that part of the air spread by the feathers passes through the wing surface, the projection area in the upwelling process is reduced through the bending of the wings in the wingspan direction, and the air resistance in the upwelling is reduced, and in the downwelling process, the wings are fully spread, the wing surface area is increased, and the flight lift is increased, so that the lift-drag ratio [14] of the wings is improved.

Flapping-wing flight is different from the traditional fixed-wing flight in that the lift and drag generated during the flapping of the wings are constantly changing, and in different flapping stages, the flapping angle of attack needs to be adjusted according to the wind direction in order to obtain the best aerodynamic characteristics. In the flapping process, because the wing has certain flexibility, the inner wing part which is close to the body has greater rigidity and smaller angle of attack. The outer wing is mainly covered by feathers and has a certain degree of free movement, so the angle of attack of the outer wing changes greatly during flight [15–17]. Figure 2 shows the aerodynamic characteristics of the inner wing at different angles of attack during the upstroke and downstroke motions. The relative velocity of the wing is the resultant velocity of the flight velocity and the wing flapping velocity, and the resultant aerodynamic force generated by the wing during flight is perpendicular to the relative velocity.

3. Establishment of Flapping-Wing Flight Dynamics Model

3.1. Definition of Coordinate System of Flapping-Wing Flight Motion Model. In the flapping-wing flight process, the center of mass and the moment of inertia of the whole flight system will change due to the flapping up and down of the flapping wing, and the center of mass and the moment of inertia of the flight system are time-varying functions. Therefore, it is necessary to describe the motion equations of each part of the flapping-wing flight system separately [18]. When describing the motion model of the system, the motion parameters of each component are described in the same coordinate system through coordinate transformation. For this reason, according to the needs of flapping-wing flight, a ground coordinate system ($OX_eY_eZ_e$), flight path coordinate system ($ox_ky_kz_k$), velocity coordinate system ($ox_ay_az_a$), fuselage coordinate system ($ox_by_bz_b$), and wing coordinate system ($ox_wy_wz_w$) are shown in Figure 3.

3.2. Analysis of Aerodynamic Parameters of Flapping Wing. Before establishing the mathematical model of flapping-wing flight kinematics and dynamics, it is necessary to analyze the forces acting on the fuselage and wing during flapping-wing flight. Flapping wing is a complex multi-input and multi-output nonlinear system, and it is affected by many external and internal disturbance factors during its flight [19]. Therefore, in the aerodynamic analysis of the flapping wing, the following assumptions are made for the bionic flapping-wing model [20]:

(a) The mass and motion characteristics of each component of the bionic flapping-wing system are measurable and constant.

(b) The wings on both sides flutter symmetrically around the axis of the fuselage, and the flapping speed is constant.

(c) The change in the center of gravity and the moment and product of inertia of the system due to the mass of the wing during flapping is not considered.

(d) The system is rigid with no flexible deformation and uniform mass distribution.

The flapping-wing flight system can be divided into two parts: the fuselage and the wing. The wing is the main source of lift needed for flight, while the fuselage generates part of the lift and bears the air resistance. Therefore, when analyzing the aerodynamic parameters of the flapping-wing system, these two parts are mainly analyzed.

3.2.1. Force and Moment Analysis of Fuselage

(1) Fuselage Force. During flapping-wing flight, there are three main external forces on the fuselage: gravity **G**, external aerodynamic force **Q**, and the force **T** exerted on the fuselage by the flapping wing, as shown in Figure 4.

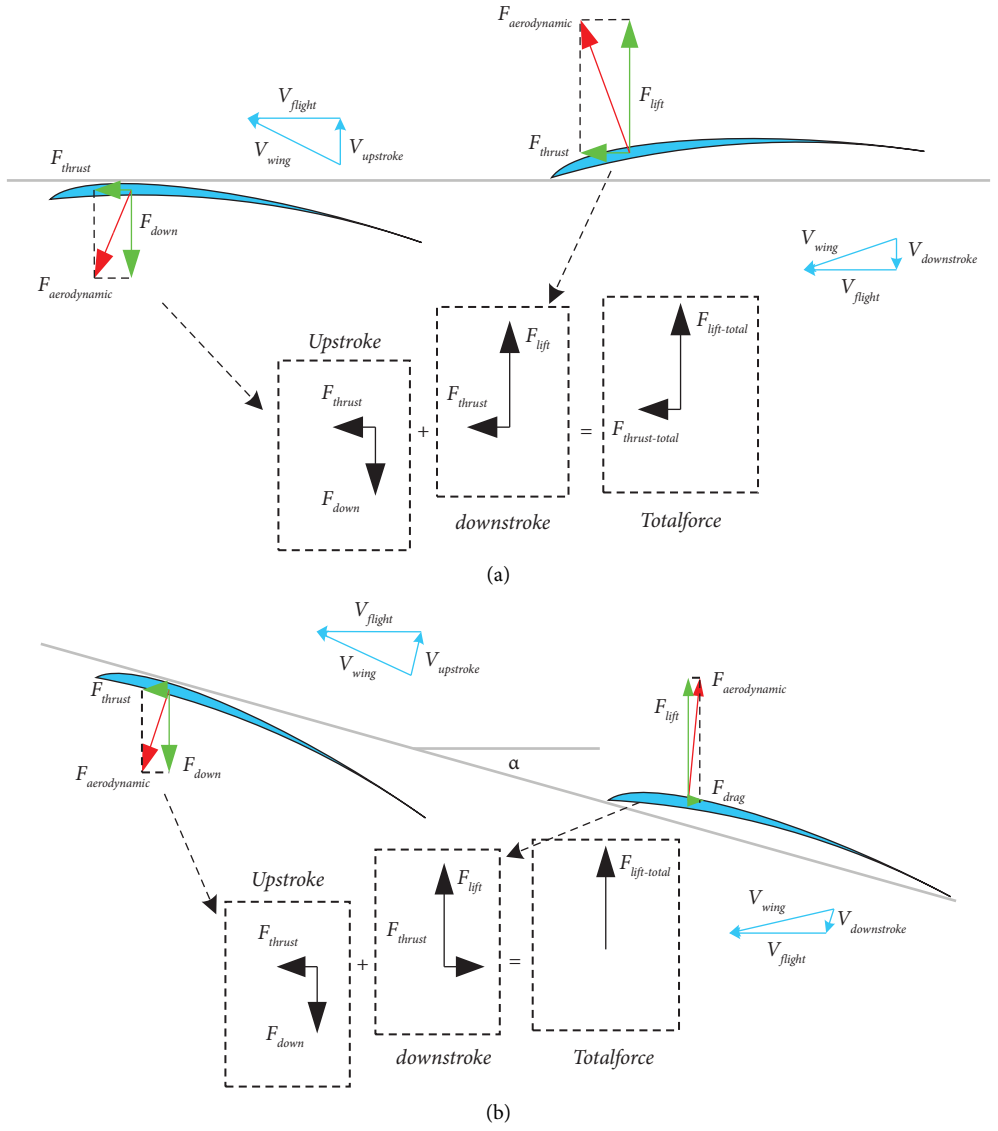

FIGURE 2: Analysis of aerodynamic forces generated by wing flapping during flapping flight. (a) Analysis of aerodynamic forces generated by wing flapping when the flight angle of attack $\alpha = 0^{\circ}$. (b) Analysis of aerodynamic forces generated by wing flapping when the flight angle of attack $\alpha \neq 0^{\circ}$.

During flapping flight, the aerodynamic force acting on the fuselage is proportional to the flight speed, air density, and windward area of the fuselage, so the aerodynamic force can be expressed as

$$Q = \frac{1}{2} C_v \rho V^2 S_b, \tag{1}$$

where C_v is a dimensionless coefficient, ρ is the air density, S_b is the windward area of the fuselage, and V is the fuselage speed.

The aerodynamic force acting on the fuselage can be decomposed into the drag force along the ox_a direction, the lift force along the oy_a direction, and the side force along the oz_a direction in the velocity coordinate system, which can be expressed as

$$\begin{bmatrix} Q_{xa} \\ Q_{ya} \\ Q_{za} \end{bmatrix} = \begin{bmatrix} \frac{1}{2} C_{xv} \rho S_b V^2 \\ \frac{1}{2} C_{yv} \rho S_b V^2 \\ \frac{1}{2} C_{zv} \rho S_b V^2 \end{bmatrix}, \tag{2}$$

where C_{xv}, C_{yv}, and C_{zv} are the drag, lift, and side force coefficients of the fuselage in the velocity coordinate system, respectively.

In the ground coordinate system, the gravity of the fuselage is opposite to OY_e, so it can be expressed as

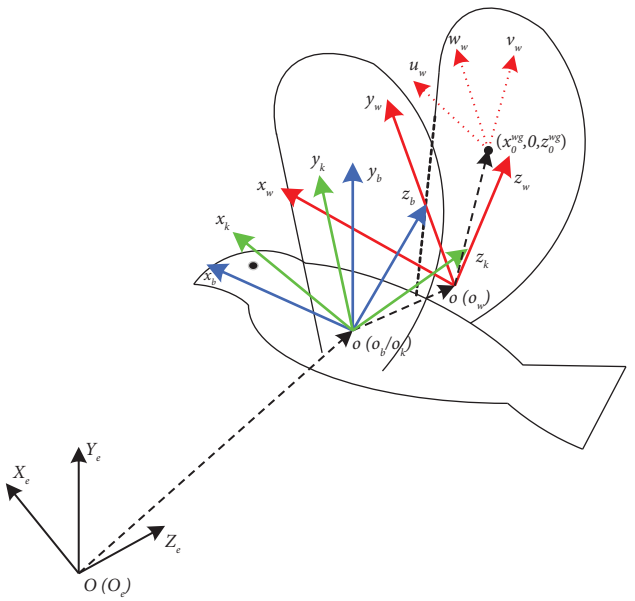

Figure 3: Flapping wing flight coordinate system definition.

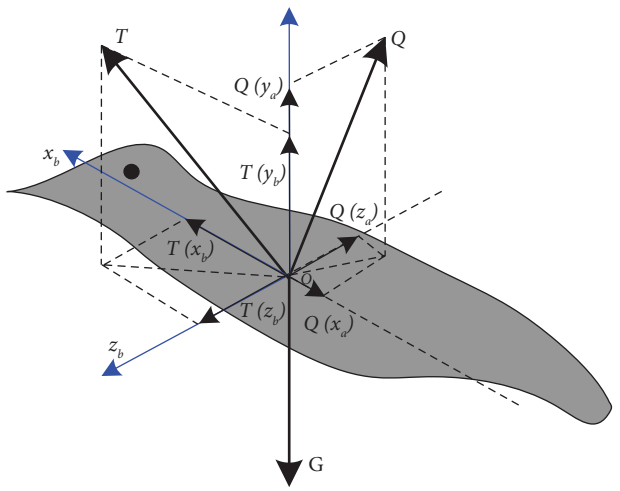

Figure 4: Forces on fuselage.

$$\begin{bmatrix} G_X \\ G_Y \\ G_Z \end{bmatrix} = \begin{bmatrix} 0 \\ -\mathrm{mg} \\ 0 \end{bmatrix}. \tag{3}$$

At the same time, the driving force generated by the wing flapping acts on the fuselage, which can be expressed in the fuselage coordinate system as

$$F_b^{\mathrm{wg}} = \begin{bmatrix} F_{\mathrm{xb}}^{\mathrm{wg}} \\ F_{\mathrm{yb}}^{\mathrm{wg}} \\ F_{\mathrm{zb}}^{\mathrm{wg}} \end{bmatrix}. \tag{4}$$

When calculating the aerodynamic forces acting on flapping flight, it is essential to transform the forces acting on the body into a common coordinate system. Based on the coordinate transformation relationships obtained earlier, the gravitational force (G), external aerodynamic forces (Q), and the propulsive force ($Fwgb$) exerted by the wings on the body are unified into the trajectory coordinate system. This enables the establishment of the motion and dynamic equations for flapping flight. According to the transformation relationships, we can derive the following:

$$\begin{aligned} \begin{bmatrix} Q_{\mathrm{xk}} \\ Q_{\mathrm{yk}} \\ Q_{\mathrm{zk}} \end{bmatrix} &= \mathrm{L}_a^{\mathrm{k}}(\gamma_a) \begin{bmatrix} Q_{\mathrm{xa}} \\ Q_{\mathrm{ya}} \\ Q_{\mathrm{za}} \end{bmatrix} \\ &= \begin{bmatrix} 1 & 0 & 0 \\ 0 & \cos\gamma_a & \sin\gamma_a \\ 0 & -\sin\gamma_a & \cos\gamma_a \end{bmatrix}^T \begin{bmatrix} \frac{1}{2}C_{xv}\rho S_b V^2 \\ \frac{1}{2}C_{yv}\rho S_b V^2 \\ \frac{1}{2}C_{zv}\rho S_b V^2 \end{bmatrix} \\ &= \begin{bmatrix} \frac{1}{2}C_{\mathrm{xa}}\rho S_b V^2 \\ \frac{1}{2}\rho S_b V^2\left(C_{\mathrm{ya}}\cos\gamma_a - C_{\mathrm{zv}}\sin\gamma_a\right) \\ \frac{1}{2}\rho S_b V^2\left(C_{\mathrm{ya}}\sin\gamma_a + C_{\mathrm{za}}\cos\gamma_a\right) \end{bmatrix}, \end{aligned} \tag{5}$$

where $L_a^k(\gamma_a) = [L_k^a(\gamma_a)]^T$.

$$\begin{aligned} \begin{bmatrix} G_{\mathrm{Xk}} \\ G_{\mathrm{Yk}} \\ G_{\mathrm{Zk}} \end{bmatrix} &= L_e^k(\Theta,\Psi) \begin{bmatrix} Q_{\mathrm{xk}} \\ Q_{\mathrm{yk}} \\ Q_{\mathrm{zk}} \end{bmatrix} \\ &= \begin{bmatrix} \cos\Theta\cos\Psi & \sin\Theta & -\cos\Theta\sin\Psi \\ -\sin\Theta\cos\Psi & \cos\Theta & \sin\Theta\sin\Psi \\ \sin\Psi & 0 & \cos\Psi \end{bmatrix} \begin{bmatrix} 0 \\ -\mathrm{mg} \\ 0 \end{bmatrix} \\ &= \begin{bmatrix} -\mathrm{mgsin}\Theta \\ -\mathrm{mgcos}\Theta \\ 0 \end{bmatrix}. \end{aligned} \tag{6}$$

The aerodynamic force on the wing in the flight path coordinate system is expressed as

$$\begin{aligned} \begin{bmatrix} F_{\mathrm{xk}}^{\mathrm{wg}} \\ F_{\mathrm{yk}}^{\mathrm{wg}} \\ F_{\mathrm{zk}}^{\mathrm{wg}} \end{bmatrix} &= L_a^k(\gamma_a) L_b^a(\alpha,\beta) \begin{bmatrix} F_{\mathrm{xb}}^{\mathrm{wg}} \\ F_{\mathrm{yb}}^{\mathrm{wg}} \\ F_{\mathrm{zb}}^{\mathrm{wg}} \end{bmatrix} \\ &= \begin{bmatrix} F_{\mathrm{xk}}^{\mathrm{wg}}(11) \\ F_{\mathrm{yk}}^{\mathrm{wg}}(12) \\ F_{\mathrm{zk}}^{\mathrm{wg}}(13) \end{bmatrix}, \end{aligned} \tag{7}$$

where

$$\begin{cases} F_{\mathrm{xk}}^{\mathrm{wg}}(11) = F_{\mathrm{xb}}^{\mathrm{wg}}\cos\alpha\cos\beta - F_{\mathrm{yb}}^{\mathrm{wg}}\sin\alpha\cos\beta + F_{\mathrm{zb}}^{\mathrm{wg}}\sin\beta, \\ F_{\mathrm{yk}}^{\mathrm{wg}}(12) = F_{\mathrm{xb}}^{\mathrm{wg}}\left(\sin\alpha\cos\gamma_a + \cos\alpha\sin\beta\sin\gamma_a\right) + F_{\mathrm{yb}}^{\mathrm{wg}}\left(\cos\alpha\cos\gamma_a - \sin\alpha\sin\beta\sin\gamma_a\right) \\ -F_{\mathrm{zb}}^{\mathrm{wg}}\cos\beta\sin\gamma_a, \\ F_{\mathrm{zk}}^{\mathrm{wg}}(13) = F_{\mathrm{xb}}^{\mathrm{wg}}\left(\sin\alpha\sin\gamma_a + \cos\alpha\sin\beta\cos\gamma_a\right) + F_{\mathrm{yb}}^{\mathrm{wg}}\left(\cos\alpha\sin\gamma_a + \sin\alpha\sin\beta\cos\gamma_a\right) \\ -F_{\mathrm{zb}}^{\mathrm{wg}}\cos\beta\cos\gamma_a. \end{cases} \tag{8}$$

Based on equations (5)–(8), the components of the resultant external force (F_{tot}^{b}) acting on the body in the trajectory coordinate system along each axis are as follows:

$$\begin{aligned} F_{\mathrm{tot}}^{b} &= \begin{bmatrix} F_{\mathrm{xk}}^{b} \\ F_{\mathrm{yk}}^{b} \\ F_{\mathrm{zk}}^{b} \end{bmatrix} \\ &= \begin{bmatrix} Q_{\mathrm{xk}} \\ Q_{\mathrm{yk}} \\ Q_{\mathrm{zk}} \end{bmatrix} + \begin{bmatrix} G_{Xk} \\ G_{Yk} \\ G_{Zk} \end{bmatrix} + \begin{bmatrix} F_{\mathrm{xk}}^{\mathrm{wg}} \\ F_{\mathrm{yk}}^{\mathrm{wg}} \\ F_{\mathrm{zk}}^{\mathrm{wg}} \end{bmatrix} \\ &= \begin{bmatrix} F_{\mathrm{xk}}^{b}(11) \\ F_{\mathrm{yk}}^{b}(12) \\ F_{\mathrm{zk}}^{b}(13) \end{bmatrix}, \end{aligned} \tag{9}$$

$$\begin{cases} F_{\mathrm{xk}}^{b}(11) = \dfrac{1}{2}C_{\mathrm{xa}}\rho S_b V^2 - \mathrm{mg}\quad \sin\Theta + F_{\mathrm{xb}}^{\mathrm{wg}}\cos\alpha\cos\beta - F_{\mathrm{yb}}^{\mathrm{wg}}\sin\alpha\cos\beta + F_{\mathrm{zb}}^{\mathrm{wg}}\sin\beta, \\ F_{\mathrm{yk}}^{b}(11) = \dfrac{1}{2}\rho S_b V^2\left(C_{\mathrm{ya}}\cos\gamma_a - C_{zv}\sin\gamma_a\right) - \mathrm{mg}\quad \cos\Theta + F_{\mathrm{xb}}^{\mathrm{wg}}\left(\sin\alpha\cos\gamma_a + \cos\alpha\sin\beta\sin\gamma_a\right) \\ + F_{\mathrm{yb}}^{\mathrm{wg}}\left(\cos\alpha\cos\gamma_a - \sin\alpha\sin\beta\sin\gamma_a\right) - F_{\mathrm{zb}}^{\mathrm{wg}}\cos\beta\sin\gamma_a, \\ F_{\mathrm{zk}}^{b}(11) = \dfrac{1}{2}\rho S_b V^2\left(C_{\mathrm{ya}}\sin\gamma_a + C_{\mathrm{za}}\cos\gamma_a\right) + F_{\mathrm{xb}}^{\mathrm{wg}}\left(\sin\alpha\sin\gamma_a + \cos\alpha\sin\beta\cos\gamma_a\right) \\ + F_{\mathrm{yb}}^{\mathrm{wg}}\left(\cos\alpha\sin\gamma_a + \sin\alpha\sin\beta\cos\gamma_a\right) - F_{\mathrm{zb}}^{\mathrm{wg}}\cos\beta\cos\gamma_a. \end{cases}$$

(2) Moment Acting on the Fuselage. The force acting on the fuselage will produce a moment on the fuselage, which will change the posture of the fuselage. In the velocity frame, the body moment can be expressed as

$$M_b = \frac{1}{2}\rho C_{\mathrm{m}} V^2 S_b \delta. \tag{10}$$

The pitching, yawing, and rolling moments in the velocity coordinate can be obtained by decomposing the fuselage moments along the three directions as follows:

$$\begin{bmatrix} M_{\mathrm{ax}} \\ M_{\mathrm{ay}} \\ M_{\mathrm{az}} \end{bmatrix} = \begin{bmatrix} \frac{1}{2}\rho C_{\mathrm{mx}} V^2 S_b \delta_x \\ \frac{1}{2}\rho C_{\mathrm{my}} V^2 S_b \delta_y \\ \frac{1}{2}\rho C_{\mathrm{mz}} V^2 S_b \delta_z \end{bmatrix}, \tag{11}$$

where C_{mx}, C_{my}, and C_{mz} represent the rolling moment coefficient, yawing moment coefficient, and pitching moment coefficient, respectively, and δ_x, δ_y, and δ_z are the corresponding characteristic lengths for calculating the rolling moment, yawing moment, and pitching moment. $\delta_x = \delta_y = R$, $\delta_z = 0.25\mathrm{c}$.

According to the conversion relationship between the velocity coordinate system and the fuselage coordinate system, the fuselage moment under the velocity coordinate system can be converted into the fuselage coordinate system, and the conversion relationship is as follows:

$$\begin{aligned} M_b &= L_a^b(\alpha, \beta) \begin{bmatrix} M_{\mathrm{ax}} \\ M_{\mathrm{ay}} \\ M_{\mathrm{az}} \end{bmatrix} \\ &= \begin{bmatrix} \cos\alpha\cos\beta & \sin\alpha & -\cos\alpha\sin\beta \\ -\sin\alpha\cos\beta & \cos\alpha & \sin\alpha\sin\beta \\ \sin\beta & 0 & \cos\beta \end{bmatrix} \begin{bmatrix} \frac{1}{2}\rho C_{\mathrm{mx}} V^2 S_b \delta_x \\ \frac{1}{2}\rho C_{\mathrm{my}} V^2 S_b \delta_y \\ \frac{1}{2}\rho C_{\mathrm{mz}} V^2 S_b \delta_z \end{bmatrix} \\ &= \begin{bmatrix} \frac{1}{2}\rho V^2 S_b \left(\delta_x C_{\mathrm{mx}} \cos\alpha\cos\beta + \delta_y C_{\mathrm{my}} \sin\alpha - \delta_z C_{\mathrm{mz}} \cos\alpha\sin\beta\right) \\ \frac{1}{2}\rho V^2 S_b \left(-\delta_x C_{\mathrm{mx}} \sin\alpha\cos\beta + \delta_y C_{\mathrm{my}} \cos\alpha + \delta_z C_{\mathrm{mz}} \sin\alpha\sin\beta\right) \\ \frac{1}{2}\rho V^2 S \left(\delta_x C_{\mathrm{mx}} \sin\beta + \delta_z C_{\mathrm{mz}} \cos\beta\right) \end{bmatrix}. \end{aligned} \tag{12}$$

3.2.2. Determination of Wing Aerodynamic Parameters

(1) Wing Force. In flapping-wing flight, the motion of the wing produces lift F_L^{wg} and resistance F_D^{wg}. At the same time, due to the friction between the wing and the air in the flapping process, friction F_f^{wg} will be generated. When the wing is flapping, there is also an inertial force F_I^{wg}. Because the flapping wing can realize the up-and-down flapping motion and the chord-wise twisting motion, the change of the motion mode in the flapping process can also cause the wake flow to compensate the force. Therefore, the resultant of the instantaneous aerodynamic forces acting on the wing as it flutters can be written as

$$F_{\mathrm{tot}}^{\mathrm{wg}} = F_f^{\mathrm{wg}} + F_I^{\mathrm{wg}} + F_L^{\mathrm{wg}} + F_D^{\mathrm{wg}} + \mathrm{F}_{\mathrm{wc}}^{\mathrm{wg}}. \tag{13}$$

The wing of the flapping-wing flight platform adopts a light flexible smooth wing surface, the friction coefficient of the wing surface is very small, and the friction force generated between the wing surface and the air in the flapping process is very small. The mass of the wing is not taken into account before the external force is applied to the flapping wing, so the inertial force of the wing can also be ignored when the wing is flapping. Compared with the whole flapping-wing system, the mass of the flapping-wing flight platform made of lightweight materials can also be ignored. The twist angle of the designed wing is small, and the change of the flapping-wing motion state is small, so the wake capture force is small and can be ignored. The instantaneous aerodynamic forces acting on the wing in this way can be simplified as

$$\mathrm{F}_{\mathrm{tot}}^{\mathrm{wg}} = \mathrm{F}_{L}^{\mathrm{wg}} + \mathrm{F}_{D}^{\mathrm{wg}}. \tag{14}$$

As shown in Figure 5, the instantaneous aerodynamic force acting on the wing is mainly composed of lift and drag, which can be expressed in the wing coordinate system as

$$F_{L}^{\mathrm{wg}} = \frac{1}{2}\rho V_{w}^{2} C_{L} \int_{0}^{R} c(r)\mathrm{d}r, \tag{15}$$

$$F_{D}^{\mathrm{wg}} = \frac{1}{2}\rho V_{w}^{2} C_{D} \int_{0}^{R} c(r)\mathrm{d}r. \tag{16}$$

In the wing coordinate system, the center of pressure of the wing is assumed to be $(x_0^{\mathrm{wg}}, 0, z_0^{\mathrm{wg}})$; convert it to the fuselage coordinate system and calculate it by time, and the velocity vector of the pressure center in the fuselage coordinate system can be obtained as

$$\begin{aligned}\begin{bmatrix} \mathrm{V}_{\mathrm{bx}_0}^{\mathrm{wg}} \\ \mathrm{V}_{\mathrm{by}_0}^{\mathrm{wg}} \\ \mathrm{V}_{\mathrm{bz}_0}^{\mathrm{wg}} \end{bmatrix} &= \frac{\mathrm{d}}{\mathrm{dt}}\left(\begin{bmatrix} \cos\varphi & -\sin\varphi & 0 \\ \sin\varphi\cos\Phi & \cos\varphi\cos\Phi & \sin\Phi \\ -\sin\varphi\sin\Phi & -\sin\Phi\cos\varphi & \cos\Phi \end{bmatrix} \begin{bmatrix} \mathrm{x}_0^{\mathrm{wg}} \\ 0 \\ \mathrm{z}_0^{\mathrm{wg}} \end{bmatrix} \right) \\ &= \begin{bmatrix} -\mathrm{x}_0^{\mathrm{wg}}\dot{\varphi}\sin\varphi \\ \mathrm{x}_0^{\mathrm{wg}}\dot{\varphi}\cos\varphi\cos\Phi - \mathrm{x}_0^{\mathrm{wg}}\dot{\Phi}\sin\varphi\sin\Phi + \mathrm{z}_0^{\mathrm{wg}}\dot{\Phi}\cos\Phi \\ -\mathrm{x}_0^{\mathrm{wg}}\dot{\varphi}\cos\varphi\sin\Phi - \mathrm{x}_0^{\mathrm{wg}}\dot{\Phi}\sin\varphi\cos\Phi - \mathrm{z}_0^{\mathrm{wg}}\dot{\Phi}\sin\Phi \end{bmatrix}. \end{aligned} \tag{17}$$

In the formula, $\mathrm{x}_0^{\mathrm{wg}} = 0.25c$ and $z_0^{\mathrm{wg}} = 0.7R$.

The components of the fuselage velocity V in the three directions on the fuselage coordinate system can be expressed as

$$\begin{bmatrix} V_{\mathrm{bx}} \\ V_{\mathrm{by}} \\ V_{\mathrm{bz}} \end{bmatrix} = \begin{bmatrix} V\cos\alpha\cos\beta \\ -V\sin\alpha\cos\beta \\ V\sin\beta \end{bmatrix}. \tag{18}$$

From (14) and (15), the velocity of the wing center of pressure in the body coordinate system is

$$\begin{aligned}\mathrm{V}_{\mathrm{b}}^{\mathrm{wg}} = \begin{bmatrix} V_{\mathrm{bx}}^{\mathrm{wg}} \\ V_{\mathrm{by}}^{\mathrm{wg}} \\ V_{\mathrm{bz}}^{\mathrm{wg}} \end{bmatrix} &= \begin{bmatrix} V_{bx_0}^{\mathrm{wg}} \\ V_{by_0}^{\mathrm{wg}} \\ V_{bz_0}^{\mathrm{wg}} \end{bmatrix} + \begin{bmatrix} V_{\mathrm{bx}} \\ V_{\mathrm{by}} \\ V_{\mathrm{bz}} \end{bmatrix} \\ &= \begin{bmatrix} V\cos\alpha\cos\beta - x_0^{\mathrm{wg}}\dot{\varphi}\sin\varphi \\ -V\sin\alpha \quad \cos\beta + x_0^{\mathrm{wg}}\dot{\varphi}\cos\varphi\cos\Phi - x_0^{\mathrm{wg}}\dot{\Phi}\sin\varphi\sin\Phi + z_0^{\mathrm{wg}}\dot{\Phi}\cos\Phi \\ V\sin\beta - x_0^{\mathrm{wg}}\dot{\varphi}\cos\varphi\sin\Phi - x_0^{\mathrm{wg}}\dot{\Phi}\sin\varphi\cos\Phi - z_0^{\mathrm{wg}}\dot{\Phi}\sin\Phi \end{bmatrix}. \end{aligned} \tag{19}$$

Then, the aerodynamic force generated during the flapping of the wing can be known as

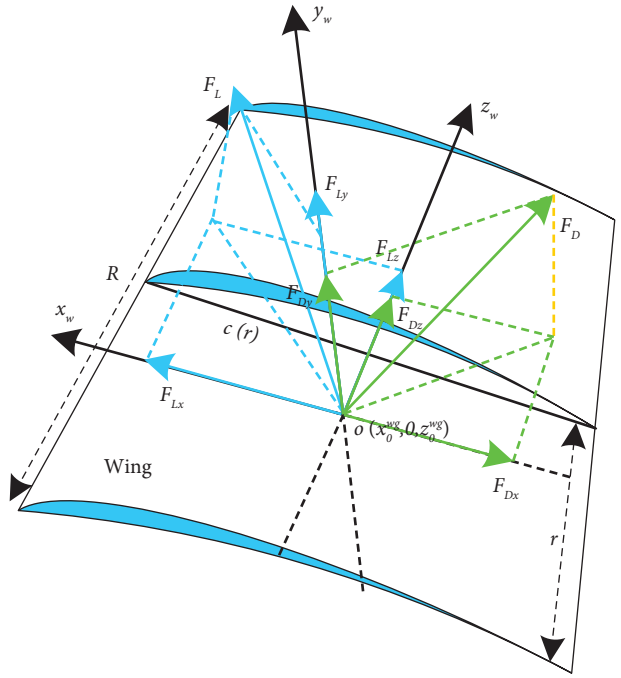

Figure 5: Instantaneous aerodynamic forces acting on the wing.

$$F_L^{wg} = \begin{bmatrix} F_{Lxb}^{wg} \\ F_{Lyb}^{wg} \\ F_{Lzb}^{wg} \end{bmatrix}$$

$$= \begin{bmatrix} \frac{1}{2}\rho V_{bx}^{wg^2} C_L \int_0^R c(r)\mathrm{d}r \\ \frac{1}{2}\rho V_{by}^{wg^2} C_L \int_0^R c(r)\mathrm{d}r \\ \frac{1}{2}\rho V_{bz}^{wg^2} C_L \int_0^R c(r)\mathrm{d}r \end{bmatrix}$$

$$= \begin{bmatrix} \frac{\rho}{2} C_L \left(V\cos\alpha\cos\beta - x_0^{wg}\dot{\varphi}\sin\varphi\right) \int_0^R c(r)\mathrm{d}r \\ \frac{\rho}{2} V_{by}^{wg^2} C_L \left(-V\sin\alpha\cos\beta + x_0^{wg}\dot{\varphi}\cos\varphi\cos\Phi - x_0^{wg}\dot{\Phi}\sin\varphi\sin\Phi + z_0^{wg}\dot{\Phi}\cos\Phi\right) \int_0^R c(r)\mathrm{d}r \\ \frac{\rho}{2} V_{bz}^{wg^2} C_L \left(V\sin\beta - x_0^{wg}\dot{\varphi}\cos\varphi\sin\Phi - x_0^{wg}\dot{\Phi}\sin\varphi\cos\Phi - z_0^{wg}\dot{\Phi}\sin\Phi\right) \int_0^R c(r)\mathrm{d}r \end{bmatrix},$$

$$
\begin{aligned}
F_D^{\mathrm{wg}} &= \begin{bmatrix} F_{\mathrm{Dxb}}^{\mathrm{wg}} \\ F_{\mathrm{Dyb}}^{\mathrm{wg}} \\ F_{\mathrm{Dzb}}^{\mathrm{wg}} \end{bmatrix} \\
&= \begin{bmatrix} \frac{1}{2}\rho V_{\mathrm{bx}}^{\mathrm{wg}^2} C_D \int_0^R c(r)\mathrm{d}r \\ \frac{1}{2}\rho V_{\mathrm{by}}^{\mathrm{wg}^2} C_D \int_0^R c(r)\mathrm{d}r \\ \frac{1}{2}\rho V_{\mathrm{by}}^{\mathrm{wg}^2} C_D \int_0^R c(r)\mathrm{d}r \end{bmatrix} \\
&= \begin{bmatrix} \frac{\rho}{2} C_D \left(V\cos\alpha\cos\beta - x_0^{\mathrm{wg}}\dot{\varphi}\sin\varphi\right) \int_0^R c(r)\mathrm{d}r \\ \frac{\rho}{2} V_{\mathrm{by}}^{\mathrm{wg}^2} C_D \left(-V\sin\alpha\cos\beta + x_0^{\mathrm{wg}}\dot{\varphi}\cos\varphi\cos\Phi - x_0^{\mathrm{wg}}\dot{\Phi}\sin\varphi\sin\Phi + z_0^{\mathrm{wg}}\dot{\Phi}\cos\Phi\right) \int_0^R c(r)\mathrm{d}r \\ \frac{\rho}{2} V_{\mathrm{bz}}^{\mathrm{wg}^2} C_D \left(V\sin\beta - x_0^{\mathrm{wg}}\dot{\varphi}\cos\varphi\sin\Phi - x_0^{\mathrm{wg}}\dot{\Phi}\sin\varphi\cos\Phi - z_0^{\mathrm{wg}}\dot{\Phi}\sin\Phi\right) \int_0^R c(r)\mathrm{d}r \end{bmatrix}.
\end{aligned} \tag{20}
$$

The total aerodynamic force $F_{\mathrm{tot}}^{\mathrm{wg}}$ due to the wing can be obtained from (17) and (18).

$$
\begin{aligned}
F_{\mathrm{tot}}^{\mathrm{wg}} &= \begin{bmatrix} F_{\mathrm{xb}}^{\mathrm{wg}} \\ F_{\mathrm{yb}}^{\mathrm{wg}} \\ F_{\mathrm{zb}}^{\mathrm{wg}} \end{bmatrix} \\
&= \begin{bmatrix} F_{\mathrm{Lxb}}^{\mathrm{wg}} \\ F_{\mathrm{Lyb}}^{\mathrm{wg}} \\ F_{\mathrm{Lzb}}^{\mathrm{wg}} \end{bmatrix} + \begin{bmatrix} F_{\mathrm{Dxb}}^{\mathrm{wg}} \\ F_{\mathrm{Dyb}}^{\mathrm{wg}} \\ F_{\mathrm{Dzb}}^{\mathrm{wg}} \end{bmatrix}.
\end{aligned} \tag{21}
$$

(2) Moment Acting on the Wing. From equation (16), the center of pressure of the wing is transformed from the wing coordinate system to the body coordinate system as

$$
\begin{bmatrix} x_{0b}^{\mathrm{wg}} \\ y_{0b}^{\mathrm{wg}} \\ z_{0b}^{\mathrm{wg}} \end{bmatrix} = \begin{bmatrix} x_0^{\mathrm{wg}}\cos\varphi \\ x_0^{\mathrm{wg}}\sin\varphi\cos\Phi + z_0^{\mathrm{wg}}\sin\Phi \\ -x_0^{\mathrm{wg}}\sin\varphi\sin\Phi + z_0^{\mathrm{wg}}\cos\Phi \end{bmatrix}. \tag{22}
$$

Assuming that the distance between the wing coordinate origin and the fuselage coordinate origin is ε, the distance between the wing pressure center and the fuselage center of mass is

$$
\begin{aligned}
l &= \begin{bmatrix} l_{\mathrm{xb}} \\ l_{\mathrm{yb}} \\ l_{\mathrm{zb}} \end{bmatrix} \\
&= \begin{bmatrix} x_{0b}^{\mathrm{wg}} \\ \mathrm{y}_{0b}^{\mathrm{wg}} \\ z_{0b}^{\mathrm{wg}} \end{bmatrix} + \begin{bmatrix} 0 \\ 0 \\ \varepsilon \end{bmatrix} \\
&= \begin{bmatrix} x_0^{\mathrm{wg}}\cos\varphi \\ x_0^{\mathrm{wg}}\sin\varphi\cos\Phi + z_0^{\mathrm{wg}}\sin\Phi \\ -x_0^{\mathrm{wg}}\sin\varphi\sin\Phi + z_0^{\mathrm{wg}}\cos\Phi + \varepsilon \end{bmatrix}.
\end{aligned} \tag{23}
$$

The moment produced by the wing is then

$$
M_w = F_{\mathrm{tot}}^{\mathrm{wg}} \times l = \begin{bmatrix} F_{\mathrm{yb}}^{\mathrm{wg}}\left(-x_0^{\mathrm{wg}}\sin\varphi\sin\Phi + z_0^{\mathrm{wg}}\cos\Phi + \varepsilon\right) + F_{\mathrm{zb}}^{\mathrm{wg}}\left(x_0^{\mathrm{wg}}\sin\varphi\cos\Phi + z_0^{\mathrm{wg}}\sin\Phi\right) \\ F_{\mathrm{xb}}^{\mathrm{wg}}\left(-x_0^{\mathrm{wg}}\sin\varphi\sin\Phi + z_0^{\mathrm{wg}}\cos\Phi + \varepsilon\right) + F_{\mathrm{zb}}^{\mathrm{wg}}x_0^{\mathrm{wg}}\cos\varphi \\ F_{\mathrm{xb}}^{\mathrm{wg}}\left(x_0^{\mathrm{wg}}\sin\varphi\cos\Phi + z_0^{\mathrm{wg}}\sin\Phi\right) + F_{\mathrm{yb}}^{\mathrm{wg}}x_0^{\mathrm{wg}}\cos\varphi \end{bmatrix}. \tag{24}
$$

During flapping-wing flight, the external gust and the airflow disturbance during flapping will affect the stability of flapping-wing flight. Therefore, it is necessary to consider the influence of the moment produced by the external disturbance force on the flapping-wing attitude when controlling the flapping-wing flight attitude. Assuming that the moment generated by the external interference force is $\mathbf{M_G}$ and the components along the body coordinate system can be expressed as M_{Gx}, M_{Gy}, and M_{Gz}, then according to the above separation, the total moment on the body is

$$
\begin{aligned}
M &= M_b + M_w + M_G \\
&= \begin{bmatrix} M_{\mathrm{bx}} \\ M_{\mathrm{by}} \\ M_{\mathrm{bz}} \end{bmatrix} + \begin{bmatrix} M_{\mathrm{wx}} \\ M_{\mathrm{wy}} \\ M_{\mathrm{wz}} \end{bmatrix} + \begin{bmatrix} M_{\mathrm{Gx}} \\ M_{\mathrm{Gy}} \\ M_{\mathrm{Gz}} \end{bmatrix} \\
&= \begin{bmatrix} M_{\mathrm{x}} \\ M_{\mathrm{y}} \\ M_{\mathrm{z}} \end{bmatrix}.
\end{aligned} \tag{25}
$$

In the formula,

$$
\begin{aligned}
M_x = {} & \frac{1}{2}\rho V^2 S_b\left(\delta_x C_{\mathrm{mx}} \cos\alpha\cos\beta + \delta_y C_{\mathrm{my}} \sin\alpha - \delta_z C_{\mathrm{mz}} \cos\alpha \sin\beta\right) \\
& + F_{\mathrm{yb}}^{\mathrm{wg}}\left(-x_0^{\mathrm{wg}} \sin\varphi \sin\Phi + z_0^{\mathrm{wg}} \cos\Phi + \varepsilon\right) + F_{\mathrm{zb}}^{\mathrm{wg}}\left(x_0^{\mathrm{wg}} \sin\varphi \cos\Phi + z_0^{\mathrm{wg}} \sin\Phi\right) + M_{\mathrm{Gx}},
\end{aligned} \tag{26}
$$

$$
\begin{aligned}
M_y = {} & \frac{1}{2}\rho V^2 S_b\left(-\delta_x C_{\mathrm{mx}} \sin\alpha\cos\beta + \delta_y C_{\mathrm{my}} \cos\alpha + \delta_z C_{\mathrm{mz}} \sin\alpha \sin\beta\right) \\
& + F_{\mathrm{xb}}^{\mathrm{wg}}\left(-x_0^{\mathrm{wg}} \sin\varphi \sin\Phi + z_0^{\mathrm{wg}} \cos\Phi + \varepsilon\right) + F_{\mathrm{zb}}^{\mathrm{wg}} x_0^{\mathrm{wg}} \cos\varphi + M_{\mathrm{Gy}},
\end{aligned} \tag{27}
$$

$$
\begin{aligned}
M_z = {} & \frac{1}{2}\rho V^2 S_b\left(\delta_x C_{\mathrm{mx}} \sin\beta + \delta_z C_{\mathrm{mz}} \cos\beta\right) + F_{\mathrm{xb}}^{\mathrm{wg}}\left(x_0^{\mathrm{wg}} \sin\varphi \cos\Phi + z_0^{\mathrm{wg}} \sin\Phi\right) \\
& + F_{\mathrm{yb}}^{\mathrm{wg}} x_0^{\mathrm{wg}} \cos\varphi + M_{\mathrm{Gz}}.
\end{aligned} \tag{28}
$$

3.3. Establishment of Flapping-Wing Dynamic Model

3.3.1. Dynamic Equation of the Center of Mass Motion of Flapping Wing. When establishing the dynamic model of the center of mass motion of the flapping-wing flight, the above established flapping-wing flight mechanics vector equation needs to be projected into the track coordinate system $ox_k y_k z_k$ to obtain the corresponding dynamic equation.

The track coordinate system $ox_k y_k z_k$ is a moving coordinate system, which has both displacement motion (its velocity is $\mathbf{V}$) and rotation motion (its angular velocity is $\mathbf{\Omega}$) relative to the ground coordinate system. A dynamic equation is established in a moving coordinate system, and the relationship between the absolute velocity of the flapping wing in flight and the implicated velocity is as follows:

$$
\frac{\mathrm{d}V}{\mathrm{d}t} = \frac{\partial \mathrm{V}}{\partial t} + \Omega \times \mathrm{V}, \tag{29}
$$

where $(\mathrm{d}V/\mathrm{d}t)$ is the absolute derivative of the velocity vector $\mathbf{V}$ in the ground coordinate system and $(\partial V/\partial t)$ is the relative derivative of the velocity vector in the track coordinate system.

The equation of motion of the center of mass in flapping flight can be expressed as

$$
\begin{aligned}
F &= m\frac{\mathrm{d}V}{\mathrm{d}t} \\
&= m\left(\frac{\partial \mathrm{V}}{\partial t} + \Omega \times V\right),
\end{aligned} \tag{30}
$$

where the projection of each vector on each axis of the track coordinate system $ox_k y_k z_k$ can be written as

$$
\begin{aligned}
\frac{\partial \mathrm{V}}{\partial t} &= \begin{bmatrix} \dfrac{\mathrm{d}V_{\mathrm{xa}}}{\mathrm{d}t} \\ \dfrac{\mathrm{d}V_{\mathrm{ya}}}{\mathrm{d}t} \\ \dfrac{\mathrm{d}V_{\mathrm{za}}}{\mathrm{d}t} \end{bmatrix}, \\
\Omega &= \begin{bmatrix} \Omega_{\mathrm{xa}} \\ \Omega_{\mathrm{ya}} \\ \Omega_{\mathrm{za}} \end{bmatrix}, \\
V &= \begin{bmatrix} V_{\mathrm{xa}} \\ V_{\mathrm{ya}} \\ V_{\mathrm{za}} \end{bmatrix}.
\end{aligned} \tag{31}
$$

According to the definition in the track coordinate system $ox_k y_k z_k$, the velocity vector $\mathbf{V}$ coincides with the axis of ox_a in the track coordinate system, so the projection component of the velocity vector in the coordinate system can be written as

$$V = \begin{bmatrix} V_{\mathrm{xa}} \\ V_{\mathrm{ya}} \\ V_{\mathrm{za}} \end{bmatrix} = \begin{bmatrix} V \\ 0 \\ 0 \end{bmatrix}. \tag{32}$$

According to equations (29) and (30), we can get

$$\Omega \times V = \begin{bmatrix} 0 & V\Omega_{\mathrm{za}} & -V\Omega_{\mathrm{ya}} \end{bmatrix}^T. \tag{33}$$

The quasi-change from the ground coordinate system to the track coordinate system requires two rotations, and the angular velocities of the two rotations are $\dot{\Psi}_V$ and $\dot{\Theta}$, respectively, so the rotation angular velocity of the track coordinate system relative to the ground coordinate system is the synthesis of the angular velocities of the two rotations. According to the transformation matrix between the two coordinate systems, we can obtain

$$\begin{bmatrix} \Omega_{\mathrm{xa}} \\ \Omega_{\mathrm{ya}} \\ \Omega_{\mathrm{za}} \end{bmatrix} = L_e^k(\Theta, \Psi) \begin{bmatrix} 0 \\ \dot{\Psi}_V \\ 0 \end{bmatrix} + \begin{bmatrix} 0 \\ 0 \\ \dot{\Theta} \end{bmatrix} = \begin{bmatrix} \dot{\Psi}_V \sin\Theta \\ \dot{\Psi}_V \cos\Theta \\ \dot{\Theta} \end{bmatrix}. \tag{34}$$

Substituting the formulas (31) and (32) into (30), the dynamic equation of the center of mass motion of the flapping flight is finally obtained as

$$\begin{bmatrix} F_{\mathrm{xk}}^b \\ F_{\mathrm{yk}}^b \\ F_{\mathrm{zk}}^b \end{bmatrix} = \begin{bmatrix} m\dfrac{\mathrm{d}V}{\mathrm{d}t} \\ mV\dfrac{\mathrm{d}\Theta}{\mathrm{d}t} \\ -mV\cos\Theta\dfrac{\mathrm{d}\Psi_V}{\mathrm{d}t} \end{bmatrix}. \tag{35}$$

In the formula, $(\mathrm{d}V/\mathrm{d}t)$ is the track tangential acceleration, $V(\mathrm{d}\Theta/\mathrm{d}t)$ is the normal acceleration of the track, $V\cos\Theta(\mathrm{d}\Psi_V/\mathrm{d}t)$ is the track DF acceleration, and F_{xk}^b, F_{yk}^b, and F_{zk}^b represent each axis component of the resultant force on the center of mass of the flapping-wing flight platform in the track coordinate system.

3.3.2. Dynamic Equation of Flapping Wing Rotating around the Center of Mass. The dynamic equation of flapping wing rotating around the center of mass is most clearly expressed in the form of scalar in the fuselage coordinate system. The body coordinate system $ox_by_bz_b$ is a moving coordinate system. It is assumed that the angular velocity of the body coordinate system relative to the ground coordinate system is $\boldsymbol{\omega}$, **H** is the moment of momentum acting on the center of mass of the body, and **M** is the moment at the center of mass. In the fuselage coordinate system, the dynamic equation of the flapping wing rotating around the center of mass is

$$\frac{\mathrm{d}H}{\mathrm{d}t} = \frac{\partial H}{\partial t} + \omega \times H = M, \tag{36}$$

where $(\mathrm{d}H/\mathrm{d}t)$ and $(\partial H/\partial t)$ are the absolute and relative derivatives of the moment of momentum, respectively.

It is assumed that i, j, and k are unit vectors along the axes of the fuselage coordinate system, respectively, and p, q, and r are the components of the rotational angular velocity ω along the axes of the fuselage coordinate system. The moment of momentum of that fuselage can be expressed as

$$H = J \cdot \omega, \tag{37}$$

where **J** is the inertia tensor, and its matrix expression is

$$J = \begin{bmatrix} J_{\mathrm{x}} & -J_{\mathrm{xy}} & -J_{\mathrm{xz}} \\ -J_{\mathrm{yx}} & J_y & -J_{\mathrm{yz}} \\ -J_{\mathrm{zx}} & -J_{\mathrm{zy}} & J_z \end{bmatrix}. \tag{38}$$

$\mathbf{J_x}$, $\mathbf{J_y}$, and $\mathbf{J_z}$ represent the moments of inertia of the flapping-wing flight platform with respect to the axes of the fuselage coordinate system, and J_{xy}, J_{yz}, and J_{zx} represent the products of inertia of the flapping-wing flight platform with respect to the axes of the fuselage coordinate system. In order to simplify the rotation equation, the product of inertia of the flapping-wing flight platform to each axis of the fuselage coordinate system is zero. Then, the components of the moment of momentum **H** along the axes of the fuselage coordinate system are

$$\begin{bmatrix} H_x \\ H_y \\ H_z \end{bmatrix} = \begin{bmatrix} J_x & 0 & 0 \\ 0 & J_y & 0 \\ 0 & 0 & J_z \end{bmatrix} \begin{bmatrix} p \\ q \\ r \end{bmatrix} = \begin{bmatrix} J_x p \\ J_y q \\ J_z r \end{bmatrix}, \tag{39}$$

$$\frac{\partial H}{\partial t} = \frac{\mathrm{d}H_x}{\mathrm{d}t} i + \frac{\mathrm{d}H_y}{\mathrm{d}t} j + \frac{\mathrm{d}H_z}{\mathrm{d}t}, \quad k = J_x \frac{\mathrm{d}p}{\mathrm{d}t} i + J_y \frac{\mathrm{d}q}{\mathrm{d}t} j + J_z \frac{\mathrm{d}r}{\mathrm{d}t} k. \tag{40}$$

From formula (38), one obtains

$$\begin{aligned}\omega \times H &= \begin{vmatrix} i & j & k \\ p & q & r \\ H_x & H_y & H_z \end{vmatrix} \\ &= \begin{vmatrix} i & j & k \\ p & q & r \\ J_x p & J_y q & J_z r \end{vmatrix} \\ &= \left(J_z - J_y\right)\mathrm{rqi} + \left(J_x - J_z\right)\mathrm{prj} + \left(J_y - J_x\right)\mathrm{qpk}.\end{aligned} \tag{41}$$

Substituting (39) and (40) into (35), the dynamic equation for the rotation of the flapping wing around the center of mass can be expressed as

$$\begin{bmatrix} J_x \dfrac{\mathrm{d}p}{\mathrm{d}t} + \left(J_z - J_y\right)\mathrm{rq} \\ J_y \dfrac{\mathrm{d}q}{\mathrm{d}t} + \left(J_x - J_z\right)\mathrm{pr} \\ J_z \dfrac{\mathrm{d}r}{\mathrm{d}t} + \left(J_y - J_x\right)\mathrm{qp} \end{bmatrix} = \begin{bmatrix} M_x \\ M_y \\ M_z \end{bmatrix}, \tag{42}$$

where M_x, M_y, and M_z are the components of the moment about the center of mass of all external forces acting on the flapping-wing flight platform on each axis of the fuselage coordinate system $ox_by_bz_b$, respectively. Formula (41) can also be written as

$$\begin{cases} \dot{p} = \dfrac{1}{J_x}\left[M_x - \left(J_z - J_y\right)\mathrm{rq}\right], \\ \dot{q} = \dfrac{1}{J_y}\left[M_y - \left(J_x - J_x\right)\mathrm{pr}\right], \\ \dot{r} = \dfrac{1}{J_z}\left[M_z - \left(J_y - J_x\right)\mathrm{qp}\right], \end{cases} \tag{43}$$

where the expressions of M_x, M_y, and M_z are shown in equations (26)–(28).

3.3.3. Kinematic Equation of the Center of Mass Motion of the Flapping Wing. The flapping-wing centroid kinematics equation describes the real-time coordinate position of flapping-wing flight. Let u, v, and w be the components of the flapping-wing velocity vector along each axis in the ground coordinate system.

$$\begin{bmatrix} u \\ v \\ w \end{bmatrix} = \begin{bmatrix} \dfrac{\mathrm{d}x}{\mathrm{d}t} \\ \dfrac{\mathrm{d}y}{\mathrm{d}t} \\ \dfrac{\mathrm{d}z}{\mathrm{d}t} \end{bmatrix}. \tag{44}$$

According to the definition of the track coordinate system $ox_ay_az_a$, the velocity vector V coincides with the ox_a axis. According to the conversion relationship between the track coordinate system and the ground coordinate system, we can get

$$\begin{aligned}\begin{bmatrix} u \\ v \\ w \end{bmatrix} &= L_e^k(\Theta, \Psi)\begin{bmatrix} V \\ 0 \\ 0 \end{bmatrix} \\ &= \begin{bmatrix} \cos\Theta\cos\Psi & \sin\Theta & -\cos\Theta\sin\Psi \\ -\sin\Theta\cos\Psi & \cos\Theta & \sin\Theta\sin\Psi \\ \sin\Psi & 0 & \cos\Psi \end{bmatrix}\begin{bmatrix} V \\ 0 \\ 0 \end{bmatrix} \\ &= \begin{bmatrix} V\cos\Theta\cos\Psi \\ V\sin\Theta \\ -V\cos\Theta\sin\Psi \end{bmatrix}.\end{aligned} \tag{45}$$

According to the above analysis, the kinematic equation of the center of mass of the flapping wing is obtained as

$$\begin{cases} \dot{x} = V\cos\Theta\cos\Psi, \\ \dot{y} = V\sin\Theta, \\ \dot{z} = -V\cos\Theta\sin\Psi. \end{cases} \tag{46}$$

3.3.4. Kinematic Equation of Flapping-Wing Center of Mass Rotation. In order to determine the attitude, change of flapping wing in space, it is necessary to establish the kinematic equation of attitude change of flapping wing relative to the ground coordinate system, that is, to establish the corresponding relationship between the derivatives of yaw angle ψ, pitch angle θ, and roll angle γ with respect to time and the components p, q, and r of angular velocity.

According to the conversion relationship between the fuselage coordinate system and the ground coordinate system,

$$\begin{bmatrix} p \\ q \\ r \end{bmatrix} = L(\gamma)L(\theta)\begin{bmatrix} 0 \\ \dot{\psi} \\ 0 \end{bmatrix} + \mathrm{L}(\gamma)\begin{bmatrix} 0 \\ 0 \\ \dot{\theta} \end{bmatrix} + \begin{bmatrix} \dot{\gamma} \\ 0 \\ 0 \end{bmatrix} = \begin{bmatrix} \dot{\psi}\sin\theta + \dot{\gamma} \\ \dot{\psi}\cos\theta\cos\gamma + \dot{\theta}\sin\gamma \\ -\dot{\psi}\cos\theta\sin\gamma + \dot{\theta}\cos\gamma \end{bmatrix} = \begin{bmatrix} 1 & \sin\theta & 0 \\ 0 & \cos\theta\cos\gamma & \sin\gamma \\ 0 & -\cos\theta\sin\gamma & \cos\gamma \end{bmatrix}\begin{bmatrix} \dot{\gamma} \\ \dot{\psi} \\ \dot{\theta} \end{bmatrix}. \tag{47}$$

After the above equation is changed, the kinematic equation of the flapping wing rotating around the center of mass is obtained:

$$\begin{bmatrix} \dot{\theta} \\ \dot{\psi} \\ \dot{\gamma} \end{bmatrix} = \begin{bmatrix} q\sin\gamma + r\cos\gamma \\ \dfrac{1}{\cos\theta}(q\cos\gamma - r\sin\gamma) \\ p - \tan\theta(q\cos\gamma - r\sin\gamma) \end{bmatrix}. \tag{48}$$

3.3.5. Dynamic Model of Flapping-Wing Flight System. According to the above analysis, the dynamic model of the whole system in flapping-wing flight can be obtained as shown in the following equation:

$$\begin{cases} \dot{V} = \dfrac{1}{m}\left(\dfrac{1}{2}C_{\mathrm{xa}}\rho S_b V^2 - \mathrm{mg} \quad \sin\Theta + F_{\mathrm{xb}}^{\mathrm{wg}}\cos\alpha\cos\beta - F_{\mathrm{yb}}^{\mathrm{wg}}\sin\alpha\cos\beta + F_{\mathrm{zb}}^{\mathrm{wg}}\sin\beta\right), \\ \dot{\Theta} = \dfrac{1}{\mathrm{mV}}\begin{pmatrix} \dfrac{1}{2}\rho S_b V^2\left(C_{\mathrm{ya}}\cos\gamma_a - C_{\mathrm{zv}}\sin\gamma_a\right) - \mathrm{mg} \quad \cos\Theta + F_{\mathrm{xb}}^{\mathrm{wg}}\left(\sin\alpha\cos\gamma_a + \cos\alpha\sin\beta\sin\gamma_a\right) \\ + F_{\mathrm{yb}}^{\mathrm{wg}}\left(\cos\alpha\cos\gamma_a - \sin\alpha\sin\beta\sin\gamma_a\right) - F_{\mathrm{zb}}^{\mathrm{wg}}\cos\beta\sin\gamma_a \end{pmatrix}, \\ \dot{\Psi}_V = -\dfrac{1}{\mathrm{mV}\cos\Theta}\begin{pmatrix} \dfrac{1}{2}\rho S_b V^2\left(C_{\mathrm{ya}}\sin\gamma_a + C_{\mathrm{za}}\cos\gamma_a\right) + F_{\mathrm{xb}}^{\mathrm{wg}}\left(\sin\alpha\sin\gamma_a + \cos\alpha\sin\beta\cos\gamma_a\right) \\ + F_{\mathrm{yb}}^{\mathrm{wg}}\left(\cos\alpha\sin\gamma_a + \sin\alpha\sin\beta\cos\gamma_a\right) - F_{\mathrm{zb}}^{\mathrm{wg}}\cos\beta\cos\gamma_a \end{pmatrix}, \\ \dot{p} = \dfrac{1}{J_x}\begin{bmatrix} \dfrac{1}{2}\rho V^2 S_b\left(\delta_x C_{\mathrm{mx}}\cos\alpha\cos\beta + \delta_y C_{\mathrm{my}}\sin\alpha - \delta_z C_{\mathrm{mz}}\cos\alpha\sin\beta\right) \\ +\backslash F_{\mathrm{yb}}^{\mathrm{wg}}\left(-x_0^{\mathrm{wg}}\sin\varphi\sin\Phi + z_0^{\mathrm{wg}}\cos\Phi + \varepsilon\right) + F_{\mathrm{zb}}^{\mathrm{wg}}\left(x_0^{\mathrm{wg}}\sin\varphi\cos\Phi + z_0^{\mathrm{wg}}\sin\Phi\right) \\ + M_{\mathrm{Gx}} - \left(J_z - J_y\right)\mathrm{rq} \end{bmatrix}, \\ \dot{q} = \dfrac{1}{J_y}\begin{bmatrix} \dfrac{1}{2}\rho V^2 S_b\left(-\delta_x C_{\mathrm{mx}}\sin\alpha\cos\beta + \delta_y C_{\mathrm{my}}\cos\alpha + \delta_z C_{\mathrm{mz}}\sin\alpha\sin\beta\right) \\ + F_{\mathrm{xb}}^{\mathrm{wg}}\left(-x_0^{\mathrm{wg}}\sin\varphi\sin\Phi + z_0^{\mathrm{wg}}\cos\Phi + \varepsilon\right) + F_{\mathrm{zb}}^{\mathrm{wg}}x_0^{\mathrm{wg}}\cos\varphi + M_{Gy} - (J_x - J_x)\mathrm{pr} \end{bmatrix}, \\ \dot{r} = \dfrac{1}{J_z}\begin{bmatrix} \dfrac{1}{2}\rho V^2 S_b\left(\delta_x C_{\mathrm{mx}}\sin\beta + \delta_z C_{\mathrm{mz}}\cos\beta\right) + F_{\mathrm{xb}}^{\mathrm{wg}}\left(x_0^{\mathrm{wg}}\sin\varphi\cos\Phi + z_0^{\mathrm{wg}}\sin\Phi\right) \\ + F_{\mathrm{yb}}^{\mathrm{wg}}x_0^{\mathrm{wg}}\cos\varphi + M_{\mathrm{Gz}} - \left(J_y - J_x\right)\mathrm{qp} \end{bmatrix}, \\ \dot{x} = V\cos\Theta\cos\Psi, \\ \dot{y} = V\sin\Theta, \\ \dot{z} = -V\cos\Theta\sin\Psi, \\ \dot{\theta} = q\sin\gamma + r\cos\gamma, \\ \dot{\psi} = \dfrac{1}{\cos\theta}(q\cos\gamma - r\sin\gamma), \\ \dot{\gamma} = p - \tan\theta(q\cos\gamma - r\sin\gamma). \end{cases} \tag{49}$$

4. L1 Adaptive Control of Bionic Flapping-Wing Flight

In flapping-wing flight, the simplified flapping-wing flight dynamics model is shown in equation (50), assuming that the body sideslip angle is $\beta = 0^{\circ}$.

$$\begin{cases} J_x \dfrac{\mathrm{d}p}{\mathrm{d}t} + \left(J_z - J_y\right)\mathrm{rq} = M_x^b + M_x^{\mathrm{wg}} + M_x^I + M_x^G, \\ J_y \dfrac{\mathrm{d}q}{\mathrm{d}t} + \left(J_x - J_z\right)\mathrm{pr} = M_y^b + M_y^{\mathrm{wg}} + M_y^I + M_y^G, \\ J_z \dfrac{\mathrm{d}r}{\mathrm{d}t} + \left(J_y - J_x\right)\mathrm{qp} = M_z^b + M_z^{\mathrm{wg}} + M_z^I + M_z^G, \\ \dfrac{\mathrm{d}\theta}{\mathrm{d}t} = q\sin\gamma + r\cos\gamma, \\ \dfrac{\mathrm{d}\psi}{\mathrm{d}t} = \dfrac{1}{\cos\theta}\left(q\cos\gamma - r\sin\gamma\right), \\ \dfrac{\mathrm{d}\gamma}{\mathrm{d}t} = p - \tan\theta\left(q\cos\gamma - r\sin\gamma\right). \end{cases} \tag{50}$$

In the equations, M_x^b, M_y^b, and M_z^b represent the body moments of the flapping wing in three directions, while. M_x^{wg}, M_y^{wg}, and M_z^{wg} denote the roll, yaw, and pitch moments generated by wing flapping during flapping flight, with their specific expressions given in equations (51)~(52). $\mathbf{M_x^I}$, M_y^I, and M_z^I represent the systematic uncertainty vectors, respectively. M_x^G, M_y^G, and M_z^G represent the disturbances from external factors during flapping flight, such as gusts and turbulence, affecting the wing's attitude control model, and when the disturbance is used for constructing a system simulation model, an incoming flow wind resistance function is applied to the system to simulate the influence of the gust on the flapping-wing attitude in the flapping-wing flight process.

$$\begin{aligned} M^b &= \begin{bmatrix} M_x^b \\ M_y^b \\ M_z^b \end{bmatrix} \\ &= \begin{bmatrix} \dfrac{1}{2}\rho V^2 S_b\left(\delta_x C_{\mathrm{mx}}\cos\alpha + \delta_y C_{\mathrm{my}}\sin\alpha\right) \\ -\dfrac{1}{2}\rho V^2 S_b\left(\delta_x C_{\mathrm{mx}}\sin\alpha - \delta_y C_{\mathrm{my}}\cos\alpha\right) \\ \dfrac{1}{2}\rho V^2 S_b \delta_z C_{\mathrm{mz}} \end{bmatrix}, \end{aligned} \tag{51}$$

$$\begin{aligned} M^{\mathrm{wg}} &= \begin{bmatrix} M_x^{\mathrm{wg}} \\ M_y^{\mathrm{wg}} \\ M_z^{\mathrm{wg}} \end{bmatrix} \\ &= \begin{bmatrix} -F_{\mathrm{yb}}^{\mathrm{wg}}\begin{pmatrix} x_0^{\mathrm{wg}}\sin\varphi\sin\Phi \\ -z_0^{\mathrm{wg}}\cos\Phi + \varepsilon \end{pmatrix} + F_{\mathrm{zb}}^{\mathrm{wg}}\begin{pmatrix} x_0^{\mathrm{wg}}\sin\varphi\cos\Phi \\ +z_0^{\mathrm{wg}}\sin\Phi \end{pmatrix} + M_{\mathrm{Gx}} \\ -F_{\mathrm{xb}}^{\mathrm{wg}}\begin{pmatrix} x_0^{\mathrm{wg}}\sin\varphi\sin\Phi \\ -z_0^{\mathrm{wg}}\cos\Phi + \varepsilon \end{pmatrix} + F_{\mathrm{zb}}^{\mathrm{wg}} x_0^{\mathrm{wg}}\cos\varphi + M_{\mathrm{Gy}} \\ F_{\mathrm{xb}}^{\mathrm{wg}}\begin{pmatrix} x_0^{\mathrm{wg}}\sin\varphi\cos\Phi \\ +z_0^{\mathrm{wg}}\sin\Phi \end{pmatrix} + F_{\mathrm{yb}}^{\mathrm{wg}} x_0^{\mathrm{wg}}\cos\varphi + M_{\mathrm{Gz}} \end{bmatrix}. \end{aligned} \tag{52}$$

4.1. Mathematical Description of Flapping-Wing Attitude Control System. The nonlinear equation for flapping-wing flight is given by equation (50) as:

$$\dot{X} = f(X) + g(X)U, \tag{53}$$

where $X = [x_1, x_2, x_3, x_4, x_5, x_6]^T \in R^6$ represents the state variables, and $f(X)$ and $g(X)$ are functions with respect to variable X. In order to derive the nonlinear attitude equations for flapping flight, some transformations are required for equation (50), as outlined. We define

$$R_{i\times j}(x) = \begin{bmatrix} \cos\gamma & \sin\gamma & 0 \\ -\dfrac{\sin\gamma}{\cos\theta} & \dfrac{\cos\gamma}{\cos\theta} & 0 \\ \tan\theta\sin\gamma & -\tan\theta\cos\gamma & 1 \end{bmatrix}. \tag{54}$$

Then, equation (53) can be expanded in the form

$$\begin{cases} x_1 = \theta, \\ \dot{x}_1 = R_{1\times j}(x)x_2, \\ x_2 = \dot{\theta}, \\ \dot{x}_2 = a_1x_4x_6 + a_2\left[u_\theta + \theta_{p,1}^T(t)x_2(t) + \sigma_1(t)\right], \\ x_3 = \psi, \\ \dot{x}_3 = R_{2\times j}(x)x_4, \\ x_4 = \dot{\psi}, \\ \dot{x}_4 = a_3x_2x_6 + a_4\left[u_\psi + \theta_{p,2}^T(t)x_4(t) + \sigma_2(t)\right], \\ x_5 = \gamma, \\ \dot{x}_5 = R_{3\times j}(x)x_6, \\ x_6 = \dot{\gamma}, \\ \dot{x}_6 = a_5x_2x_4 + a_6\left[u_\gamma + \theta_{p,3}^T(t)x_6(t) + \sigma_3(t)\right]. \end{cases} \tag{55}$$

In the equations, $R_{1\times j}(x)$, and $R_{2\times j}(x)$, $R_{3\times j}(x)$ represent the 1st, 2nd, and 3rd rows in the matrix, while u_θ, u_ψ and u_γ are the control inputs of the system. $\theta_{p,1}^T(t) \in R^2$ for $i = 1, 2, 3$, where the two-dimensional elements represent the unmodeled dynamics related to the wing's flapping-induced self-oscillation and aerodynamic changes due to wing flexibility during flapping flight. $\sigma_i(t)$ represents external disturbances caused by gusts and oncoming flow.

The control input of the system can be expressed as

$$\begin{cases} u_\theta = F_{\text{xb}}^{\text{wg}}\left(x_0^{\text{wg}}\sin\varphi\cos\Phi + z_0^{\text{wg}}\sin\Phi\right) + F_{\text{yb}}^{\text{wg}}x_0^{\text{wg}}\cos\varphi, \\ u_\psi = F_{\text{xb}}^{\text{wg}}\left(-x_0^{\text{wg}}\sin\varphi\sin\Phi + z_0^{\text{wg}}\cos\Phi + \varepsilon\right) + F_{\text{zb}}^{\text{wg}}x_0^{\text{wg}}\cos\varphi, \\ u_\gamma = F_{\text{yb}}^{\text{wg}}\left(-x_0^{\text{wg}}\sin\varphi\sin\Phi + z_0^{\text{wg}}\cos\Phi + \varepsilon\right) + F_{\text{zb}}^{\text{wg}}\left(x_0^{\text{wg}}\sin\varphi\cos\Phi + z_0^{\text{wg}}\sin\Phi\right). \end{cases} \tag{56}$$

In (56), a_i, $i = 1, 2, \ldots, 6$. The normalization parameter can be expressed in the form

$$\begin{cases} a_1 = \dfrac{\left(J_x - J_y\right)}{J_z}, \quad a_2 = \dfrac{1}{J_z}, \\ a_3 = \dfrac{\left(J_z - J_x\right)}{J_y}, \quad a_4 = \dfrac{1}{J_y}, \\ a_5 = \dfrac{\left(J_y - J_z\right)}{J_x}, \quad a_6 = \dfrac{1}{J_x}. \end{cases} \tag{57}$$

4.2. L1 Adaptive Control Theory Analysis. The L1 adaptive control method is based on the model reference adaptive control algorithm, and a low-pass filter is added to the control input to filter out the high-frequency interference signal. It has the advantages of automatically adjusting the control according to the parameter change of the control object and has the advantages of resisting high-frequency interference. It is a fast and robust control method. The L1 adaptive system consists of four parts: controlled object, state observer, adaptive law, and control law, and its system structure is shown in Figure 6. The L1 adaptive control design of controlled objects with time-varying unknown parameter vectors is emphasized.

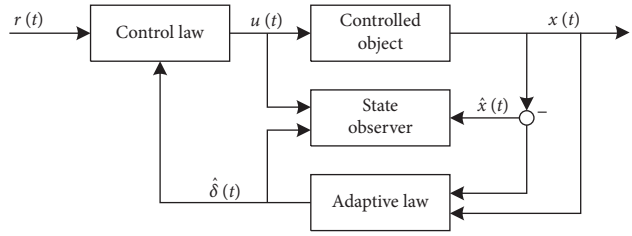

Figure 6: Structure of L1 adaptive control system.

Controlled objects are described in the form of state space, that is,

$$\begin{cases} \dot{x}(t) = Ax(t) + b\left[u(t) + \delta^T(t)x(t)\right], \\ y(t) = c^T x(t), \end{cases} \tag{58}$$

where $x(t)$ is the observable system state vector; $u(t)$ is the control vector; $\delta(t)$ is a time-varying unknown parameter vector; $y(t)$ is the output vector; and c is the system output matrix.

$$u(t) = u_1(t) - h^T x(t). \tag{59}$$

The vector $\mathbf{h}$ is designed so that $\mathbf{A_m}$ is the Hurwitz matrix, whose expression is

$$A_m = A - \mathrm{bh}^T. \tag{60}$$

According to the above formula, the controlled object (58) can be simplified as

$$\dot{x}(t) = A_m x(t) + b\left[u_1(t) + \delta^T(t)x(t)\right]. \tag{61}$$

Design state observer:

$$\dot{\hat{x}}(t) = A\hat{x}(t) + b\left[u(t) + \hat{\delta}^T(t)x(t)\right], \tag{62}$$

where $\hat{x}(t)$ and $\hat{\delta}(t)$ are the estimates of $x(t)$ and $\delta(t)$, respectively.

According to the error value between the estimated value and the actual value measured by the state observer, the adaptive law is designed:

$$\dot{\hat{\delta}}(t) = \Gamma\mathrm{Proj}\left[\hat{\delta}(t), -x(t)\tilde{x}^T(t)\mathrm{Pb}\right], \tag{63}$$

where Γ is the adaptive gain of the system; $\tilde{x}(t) = \hat{x}(t) - x(t)$; P is a positive definite symmetric matrix and satisfies $A_m^T P + \mathrm{PA}_m = -\mathrm{Q}$; Proj $(^*, ^*)$ is the projection operator; and $Q = Q^T > 0$.

Design control vector $u_1(t)$:

$$u_1(t) = C(s)\left[k_g r(t) - \hat{\delta}^T(t)x(t)\right], \tag{64}$$

where $C(s)$ is a low-pass filter; $r(t)$ is the reference input vector and has

$$k_{\mathrm{g}} = -\frac{1}{c^T A_m^{-1} b}. \tag{65}$$

When designing low-pass filter $C(s)$, the following conditions must be met:

(1) $C(s)$ is asymptotically stable and strictly regular, and the low-pass gain $C(0) = 1$.

(2) $C(s)H_0^{-1}(s)$ is stable and regular, where $H_0(s) = c^T H(s)$.

(3) $\|G(s)\|_{L_1} L < 1$, where $G(s) = H(s)[1 - C(s)]$, and $L = \max_{\delta\in\Theta}\|\delta\|_{L_1} = \max\sum_{i=1}^{n}|\delta_i|$. Θ is the given compact convex set.

4.3. Performance Index and Parameter Design of Flapping-Wing Attitude Control System. In the actual field flight test, when the flapping wing is flying, the change of its flight attitude angle changes within a certain range. According to the attitude angle change of the flapping wing in the actual flight process, the pitch angle, yaw angle, and roll angle of the airframe are limited as follows:

$$\begin{cases} 0 \le \theta \le 45^\circ, \\ 0 \le \psi \le 90^\circ, \\ 0 \le \gamma \le 30^\circ, \end{cases} \tag{66}$$

where $X = [\theta, \dot{\theta}, \psi, \dot{\psi}, \gamma, \dot{\gamma}]^T$ is a system state variable and $y = [\theta, \psi, \gamma]^T$ is the output of the system. When the flight environment and flight attitude change, the aerodynamic parameters of flapping-wing flight will be perturbed, which makes the system uncertain. $\theta_{p,1}^T(t)$ represents unmodeled dynamics of the system. At the same time, the disturbance of gust and incoming flow cannot be ignored. $\sigma_i(t)$ is an external time-varying input disturbance. Therefore, the flapping-wing attitude control system is a multi-input and multi-output nonlinear system with disturbances and uncertainties.

In the control process, the flapping-wing flight control system actually corrects the attitude angle of the flapping-wing flight in real time to ensure that the attitude angle deviation is within a reasonable range. The attitude control principle is shown in Figure 7.

When the flapping-wing flight control system is constructed, for a given initial condition and a given disturbance, the time for the system to reach the stable condition does not exceed 5 s, and the overshoot of the system does not exceed 5 degrees. It can overcome the interference of external gust, and the external wind speed is assumed to be

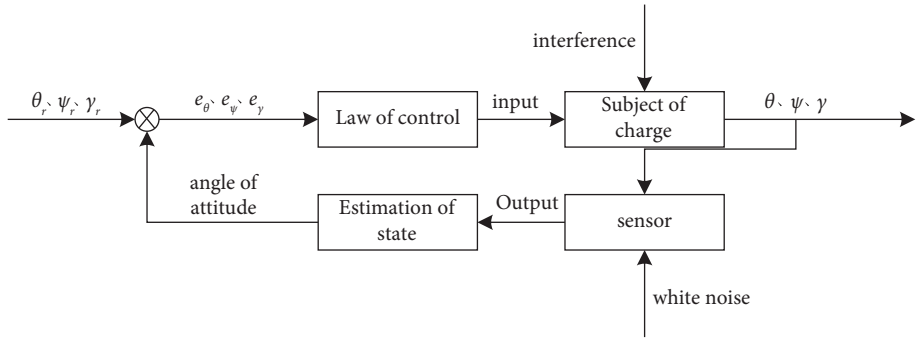

Figure 7: Schematic diagram of flapping-wing flight attitude control system.

5 m/s. Because the flight parameters of flapping-wing aircraft of different sizes are different, the parameters are only defined for the bionic flapping-wing aircraft designed by the team. At the same time, due to the different mechanical designs, system vibration, and material performance in the actual flight process, the control performance index will also change.

5. Simulation Analysis and Calculation

5.1. Flapping-Wing Attitude Control System Parameters. The parameters used in the flapping-wing attitude control system are shown in Table 1.

According to the calibration results of reference [21], the moment of inertia used in the simulation of flapping-wing flight is selected as $J_x = 112.57 \times 10^{-6}$ (kg·m^2), $J_y = 3799.3 \times 10^{-6}$ (kg·m^2), and $J_z = 3739.4 \times 10^{-6}$ (kg·m^2). Due to the differences in the shape, structure, and application environment of various kinds of flapping-wing aircraft, the design parameters of actual flapping-wing aircraft will also be different.

5.2. Construction and Simulation Analysis of Flapping-Wing Control System. According to the above analysis, the L1 adaptive attitude control system of flapping-wing flight is established. The state equation of the flapping-wing flight control system is complex. The convergence of the system is affected by many time-varying parameters. Because of the slow convergence speed of the flight state, it is necessary to constrain the input control parameters and predict the control state while establishing the flight control simulation system. Therefore, the system comprises a system dynamic model, an L1 adaptive controller, a flapping-wing flight controller, and a Monte Carlo-support vector machine parameter boundary prediction and classification module. The uncertain vector of the system is set according to the actual flying condition of the flapping wing. $\theta_{p,1}^T(t) = [\,0.2^\circ \cos t \;\; 0.15^\circ \cos t \;\; 0.1^\circ \cos t\,]^T$, the interference vector of the system $\sigma_i(t) = [\,0.3^\circ \sin t \;\; 0.2^\circ \sin t \;\; 0.1^\circ \sin t\,]^T$, flight speed $V_{ini} = 5$ m/s, setting the target flight state for the controller as $\theta_r = 0^\circ$, $\psi_r = 0^\circ$, $\gamma_r = 0^\circ$. A simulation system is established based on MATLAB2018b, and a simulation system for L1 adaptive attitude control of ornithopter is established, as shown in Figure 8.

The overall simulation of the system consists of the flapping-wing flight control simulation system based on L1AC and the predictive classification simulation of input control parameters based on Monte Carlo-support vector machine. The workflow of the complete flapping-wing aircraft simulation system is shown in Figure 8. At the beginning of the simulation, the parameters of the simulation system need to be initialized, including the system parameters of the flapping-wing aircraft, the external environment parameters, and the simulation control parameters. After the initialization is completed, the flapping wing aircraft's dynamic module is solved to obtain the minimum value of the nonlinear multivariate function, thereby obtaining the initial conditions for stable flapping flight. Linearize the system model and complete the pole placement, calculate the parameter matrix of the adaptive controller, complete the lateral and longitudinal simulation analysis of flapping-wing flight, and output the response curves of the roll, pitch, and heading of the flapping-wing vehicle with time when the target alignment is achieved, as shown in Figure 9.

Linearize the system model and complete the pole placement, calculate the parameter matrix of the adaptive controller, complete the lateral and longitudinal simulation analysis of flapping-wing flight, and output the response curves of the roll, pitch, and heading of the flapping-wing vehicle with time when the target alignment is achieved, as shown in Figure 10. From the result curve, it can be seen that the roll (γ), pitch (θ), and yaw (ψ) parameters of the L1AC controller can track the preset target values. When random interference of control variables is introduced into the simulation system, the adjustment time of pitch angle, roll angle, and yaw angle of the system is stable within 5 s, the steady-state error is small, and the overshoot after stability is small, which can meet the performance requirements of the control system. Figure 10 also presents the attitude influence curve obtained when PID controller is adopted. Compared with the attitude response curve when L1AC and PID control are adopted, it can be seen that the pitch and roll attitude of the flapping-wing aircraft cannot be stabilized within 5 s under PID control, and the overshoot of the PID control algorithm is also relatively large. By comparing the influence curves of L1AC and PID control algorithms, it can be seen that the L1AC controller designed in this paper can realize the attitude stability quickly, and the control performance is robust.

Table 1: Flapping wing design parameters.

Mass (g)	Wingspan (m)	Airfoil area (m)	Average chord length (m)	Flapping frequency (Hz)	Flutter amplitude (°)	Twist angle (°)	Flight speed ($m \cdot s^{-1}$)
500	1	0.138	0.2	5	45	10	5

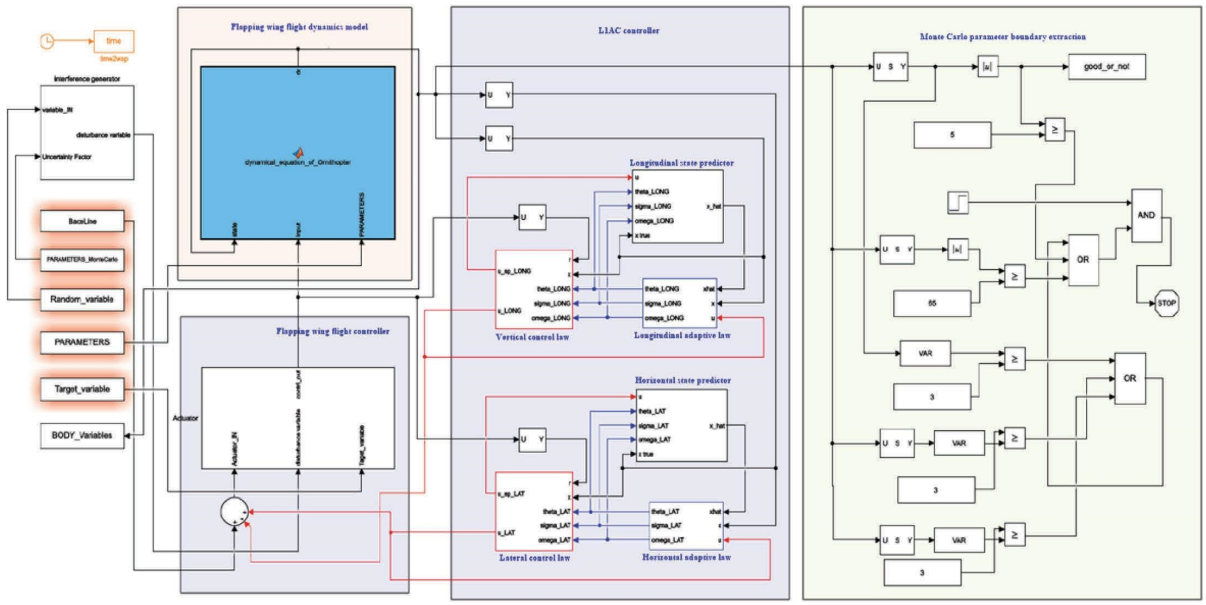

Figure 8: Block diagram of L1 adaptive attitude control system for flapping-wing flight.

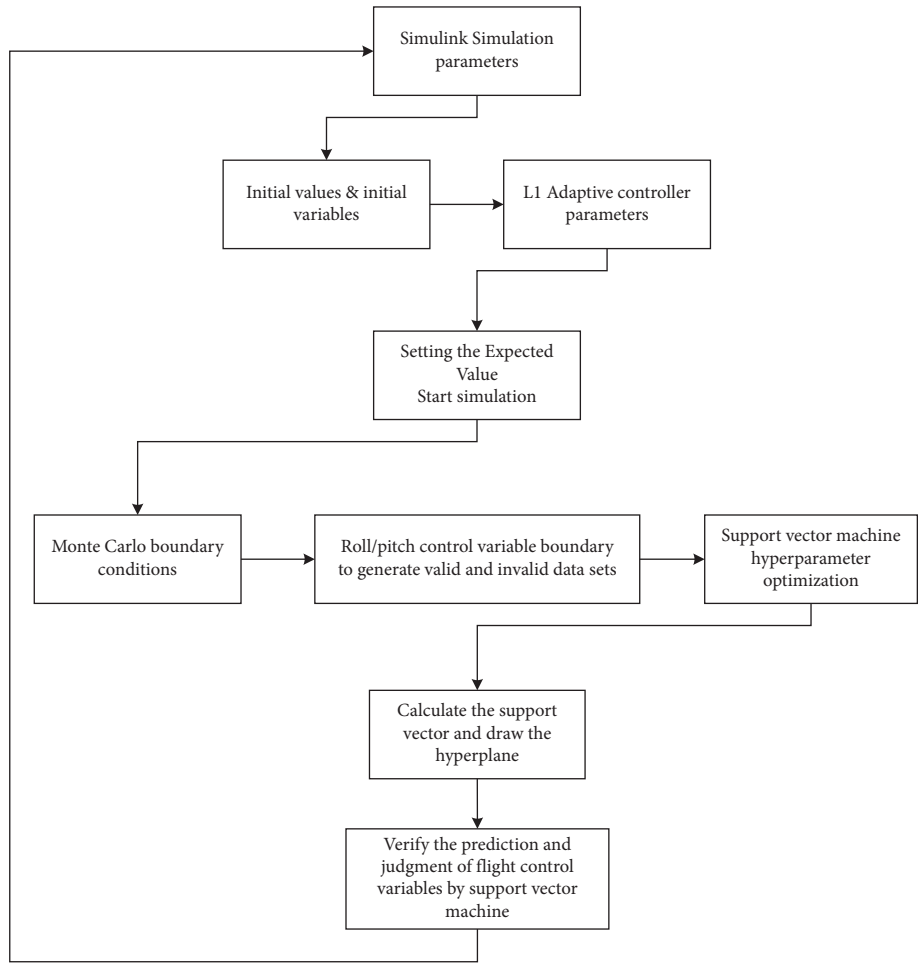

Figure 9: Simulation flow of flapping-wing attitude control system.

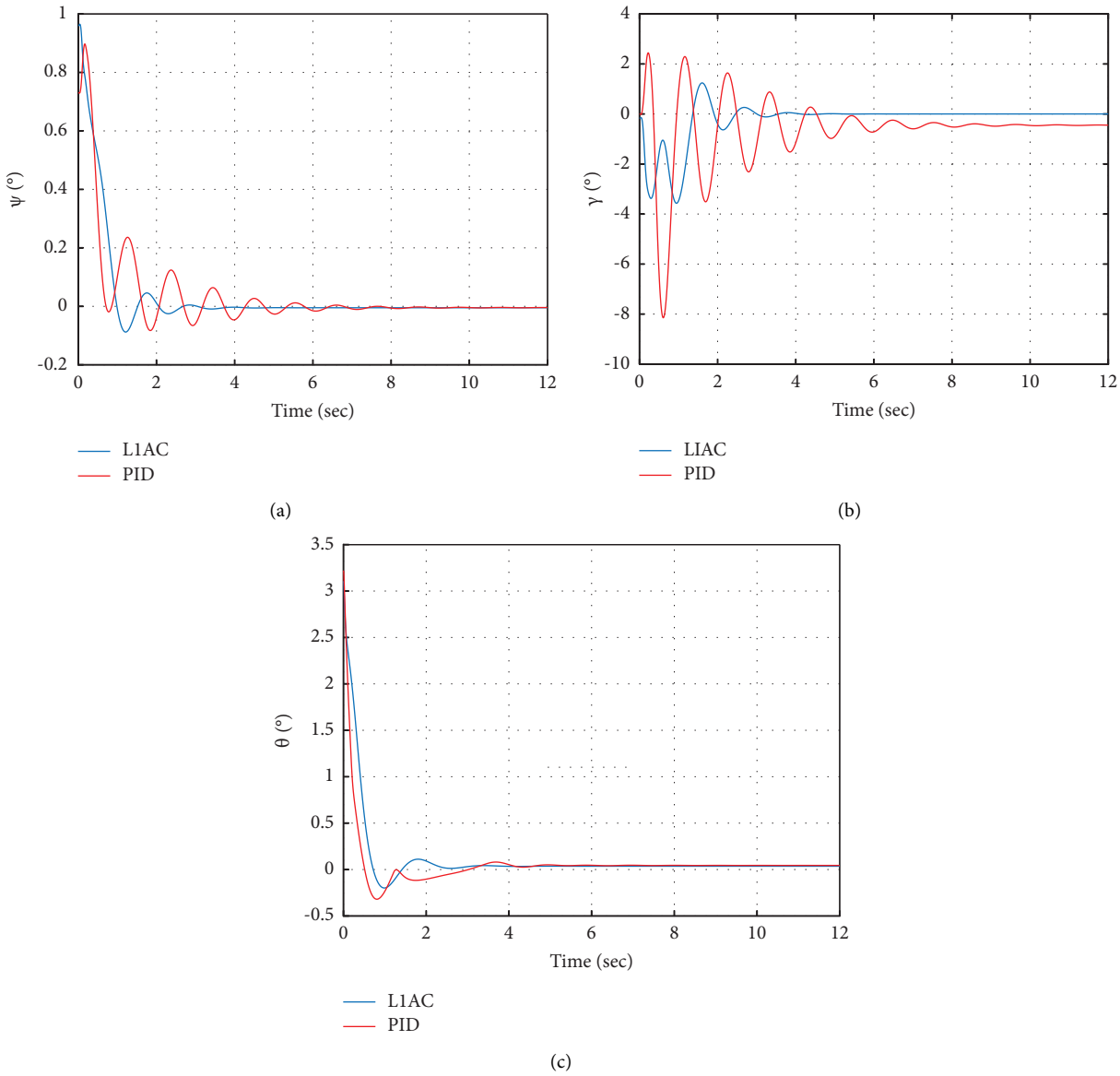

Figure 10: Response curve of flapping-wing flight attitude angle: (a) pitch angle; (b) roll angle; (c) yaw angle.

5.3. Monte Carlo-Support Vector Machine Input Control Parameter Classification Prediction. The paper proposes a Monte Carlo-support vector machine parameter boundary prediction and classification module to address the static instability of flapping-wing aircraft. This module aims to screen the control input expected variables under different flight conditions, ensuring their compliance with stable flight requirements. Random sampling is performed on the expected values of control input and various external parameter variables of flapping-wing aircraft, followed by calculating the flight status results using L1AC flight control. Statistical analysis and risk evaluation are conducted through the discriminant module for the aircraft. Control input expected variables that fail to maintain proper flight attitude or meet expectations within specified timeframes are identified as dangerous control parameters.

Considering the flight control parameter boundary optimization simulation based on Monte Carlo-support vector machine, the Monte Carlo method is used to calculate the roll (γ)/pitch (θ) variable boundary. As shown in Figure 11, the random function in MATLAB is used to perform random increment on the roll and pitch target flight states (target point), and the attitude angle is calculated through the L1AC controller. When the attitude parameter output still does not meet any of the following conditions after 14 s of calculation, the simulation is terminated:

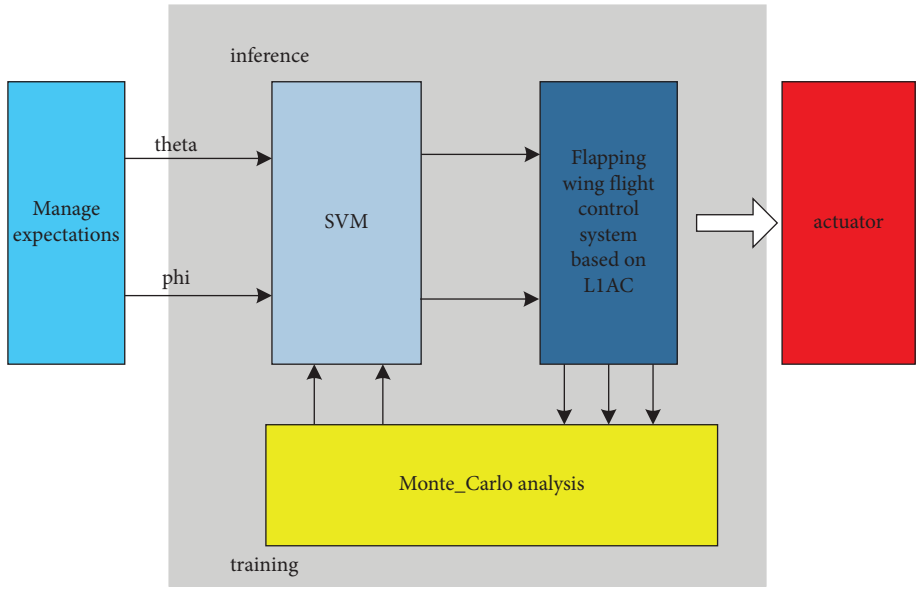

Figure 11: Classification prediction of input control parameters based on Monte Carlo-support vector machine.

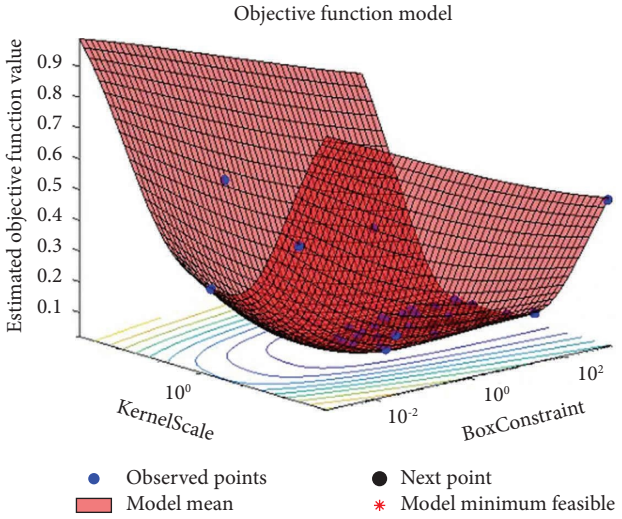

Figure 12: Objective function model.

(i) The pitch angle variance is greater than 3.

(ii) The variance of roll angle is greater than 3.

(iii) The elevation difference is greater than 5 m.

When the program enters the next iterative calculation, the pitch angle (theta), roll angle (phi), and altitude difference parameters that fail to converge beyond 14 seconds of system stabilization time are defined as exceeding the flight control redundancy limits for the control preset target point which is included in the failure parameter set, and the success dataset of system control parameters is completed in the same way. Provide a dataset basis for that classification prediction of the control parameter in the next step.

The support vector machine (SVM) module in MATLAB is used to classify and train the control input θ and γ states. Generally, after cross-validation, the kernel function parameters need to be adjusted to achieve better prediction accuracy, so the Optimize Hyperparameters variables are used to optimize the hyperparameters, and the kernel function scale parameter (Kernel Scale) and the box constraint scale are adjusted. It is convenient to find a hyperparameter that minimizes the five-fold cross-validation loss. On the one hand, the geometric sequence of box constraint parameters is tried here. Increasing the box constraint scale may reduce the number of support vectors, but it may also increase the training time. On the other hand, try a geometric sequence of RBF Sigma parameters scaled with the original kernel. Through the L1AC Simulink simulation system, in conjunction with the Monte Carlo algorithm, we generated a total of 10,000 data samples. Among these samples, 6019 input control expected variables that satisfy the normal flight safety requirements for flapping-wing

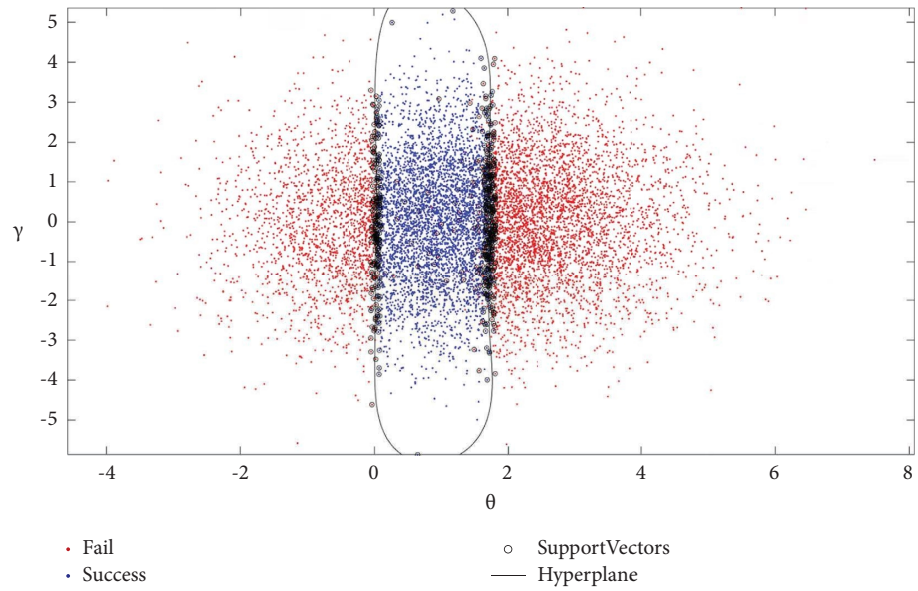

Figure 13: Positive and negative samples and hyperplanes.

aircraft were designated as positive samples, while the remaining samples were labeled as negative ones. These samples were subsequently utilized for classifier training using SVM.

The performance of SVM heavily relies on the setting of hyperparameters. Therefore, this paper employs random search to explore the range of regularization parameters and kernel function parameters within the selection set. Through iterative calculations and cross-validation, it aims to obtain a model with minimal classification error. Random search typically discovers superior hyperparameter settings within the same time frame, ultimately leading to improved results. In this study, both BoxConstraint and KernelScale parameters in SVM are constrained within the reference range [0.1 10]. The BoxConstraint parameter controls the tolerance level of the model by penalizing misclassified samples, while KernelScale parameter facilitates mapping data into a high-dimensional space for enhanced function separation. Figures 12 and 13 illustrate the constructed objective function model along with positive and negative samples as well as their corresponding hyperplane.

It can be seen that through the training of positive and negative sample sets of input expected state provided by Monte Carlo simulation and the adjustment of hyperparameters, a clear hyperplane can be found to classify and judge the target point of flapping-wing aircraft. The current results demonstrate that after 10,000 rounds of Monte Carlo simulations and 500 rounds of random search optimization, the optimal model achieved an accuracy rate of 97.97%. Furthermore, the classification accuracy reached 97.97%, with a precision rate of 96.41% and a recall rate of 98.57%. This provides a theoretical basis for the transplantation and further development of the flapping-wing flight control algorithm based on L1AC to the embedded system.

6. Conclusion

Aiming at the characteristics of bionic flapping-wing aircraft such as unsteady, strong coupling and easy to be disturbed, L1 adaptive control law is designed in this paper. Through simulation analysis, when random interference of control variables is introduced into the system, the adjustment time of pitch angle and yaw angle of the system can be stabilized within 5 s, and the rolling angle can also be stabilized within 10 s, with small control steady-state error and small overshoot after stability. It can meet the performance requirements of the control system. At the same time, the Monte Carlo-based support vector machine is used to optimize the boundary of flight control parameters. Through simulation verification, a more distinct hyperplane can be found to classify and judge the expected control parameters of the flapping-wing aircraft by inputting positive and negative sample set training and hyperparameter adjustment. The results show that the designed L1 adaptive control law has a good ability to resist the change of aircraft parameters and is robust.

The simulation results show that the L1 adaptive control law designed in this paper has good ability to resist the change of aircraft parameters and good control performance and robustness, but there are still some problems that can be further optimized. In this paper, the flight dynamics model of bionic flapping wing is constructed, assuming that the wing is rigid and the shape of the wing does not deform during flight. However, in the actual flight process of birds, the wings will produce a certain degree of flexible deformation. When the simulation model is constructed, the dynamics model of flapping-wing flight is simplified, and the influence of inertia force on flapping-wing flight is ignored. At the same time, the flight dynamics model of the whole

flapping-wing aircraft constructed in this paper and the L1 adaptive control law designed are based on theoretical derivation and simulation calculation and have not been experimentally verified on the actual bionic flapping-wing flight platform, and their reliability and usability need further research. However, the simulation results presented in this paper can provide a theoretical basis for the transplantation and further development of L1AC-based flapping-wing flight control algorithm to embedded systems.

Data Availability

The data used to support the findings of this study are included within the article.

Conflicts of Interest

The authors declare that they have no conflicts of interest.

Acknowledgments

This research was supported by the Natural Science Foundation of Shandong Province (ZR2020KF033 and ZR2023MF047), Weifang High-Tech Zone Science and Technology Benefit People Program (2021KJHM55), and Doctoral Research Start-Up Fund Project of Weifang University (2022BS22).

References

[1] T. Wang, L. I. Lei, and Q. Jiang, "DARPA fast lightweight autonomy program promotes unmanned system autonomy development," *Unmanned Systems Technology*, vol. 2, no. 1, pp. 58–64, 2019.

[2] W. He, Z. Yan, C. Sun, and Y. Chen, "Adaptive neural network control of a flapping wing micro aerial vehicle with disturbance observer," *IEEE Transactions on Cybernetics*, vol. 47, no. 10, pp. 3452–3465, 2017.

[3] B. Cheng and X. Deng, "A neural adaptive controller in flapping flight," *Journal of Robotics and Mechatronics*, vol. 24, no. 4, pp. 602–611, 2012.

[4] A. A. Rodriguez, K. Puttannaiah, and Z. Y. Lin, "Modeling, design and control of low-cost differential-drive robotic ground vehicles: Part II-Multiple vehicle study," in *Proceedings of the 2017 IEEE Conference on Control Technology and Applications (CCTA)*, Kohala Coast, HI, USA, August 2017.

[5] P. Chirarattananon, K. Y. Ma, S. B. Fuller, and R. J. Wood, "Controlled flight of a biologically inspired, insect-scale robot," *Science*, vol. 340, no. 6132, pp. 603–607, 2013.

[6] P. Chirarattananon, K. Y. Ma, and R. J. Wood, "Adaptive control of a millimeter-scale flapping-wing robot," *Bioinspiration & Biomimetics*, vol. 9, no. 2, Article ID 025004, 2014.

[7] J. E. Bluman and C. K. Kang, "Balancing the efficiency and stability of the coupled dynamics and aerodynamics of a flapping flyer," in *Proceedings of the AIAA Modeling and Simulation Technologies Conference*, Boston, MA, USA, August 2016.

[8] J. E. Bluman, C.-K. Kang, and Y. Shtessel, "Control of a flapping-wing micro air vehicle: sliding-mode approach," *Journal of Guidance, Control, and Dynamics*, vol. 41, no. 5, pp. 1223–1226, 2018.

[9] S. Tahmasian, C. A. Woolsey, and H. E. Taha, "Longitudinal flight control of flapping wing micro air vehicles," in *Proceedings of the AIAA Guidance, Navigation, & Control Conference*, Biscayne, FL, USA, August 2014.

[10] S. Tahmasian and C. A. Woolsey, "Flight control of biomimetic air vehicles using vibrational control and averaging," *Journal of Nonlinear Science*, vol. 27, no. 4, pp. 1193–1214, 2017.

[11] S. Biswal, M. Mignolet, and A. A. Rodriguez, "Modeling and control of flapping wing MicroAerial vehicles," *Bioinspiration & Biomimetics*, vol. 14, no. 2, Article ID 026004, 2019.

[12] M. Sun, "Unsteady lift mechanisms in insect flight," *Advances in mechanics*, vol. 32, no. 3, pp. 425–434, 2002.

[13] M. Sun and J. Wu, "Unsteady lift mechanisms and energetic in flying insects," *Journal of Beijing University of Aeronautics and Astronautics*, vol. 29, pp. 970–977, 2003.

[14] Ornithopters, "How ornithopters fly," 2014, http://www.ornithopter.de/english/index_en.htm.

[15] S. Dalton, *The Miracle of Flight*, Firefly Books Ltd, Richmond Hill, Canada, 1999.

[16] A. David E, *Nature's Flyers: Birds, Insects, and the Biomechanics of Flight*, The Johns Hopkins University Press, Baltimore, MD, USA, 2004.

[17] H. Greenewalt, *Crawford. Hummingbirds*, Doubleday, New York, NY, USA, 1960.

[18] A. Ramezani, X. Shi, and S.-J. Chung, "Modeling and nonlinear flight controller synthesis of a bat-inspired micro aerial vehicle," in *Proceedings of the AIAA Guidance, Navigation, and Control Conference*, Boston, MA, USA, January 2016.

[19] J. Hoff, A. Ramezani, and S. J. Chung, "Reducing versatile bat wing conformations to a1-dof machine," in *Proceedings of the 6th International Conference on Biomimetic and Biohybrid Systems*, Stanford, CA, USA, June 2017.

[20] R. Zeng, *Aerodynamic Characteristics of Flapping-wing MAV Simulating Bird Flight*, Nanjing University of Aeronautics and Astronautics, Nanjing, China, 2005.

[21] C. Cao and N. Hovakimyan, "L1 adaptive controller for nonlinear systems in the presence of unmodelled dynamics: Part II," in *Proceedings of the American Control Conference*, pp. 4099–4104, Seattle, WA, USA, June 2008.